The Quest for the Most Suitable Density Profile of the Bubble Nuclei

A thesis submitted in the partial fulfilment of the requirements for the award of

Degree of

Master of Science

In

Physics

Submitted by:

Purujeet Yadav

Roll No. 302104001

Under the Supervision

of

Dr. Soumendu Jana

Professor

School of Physics and Materials Science

THAPAR INSTITUTE
OF ENGINEERING & TECHNOLOGY
(Deemed to be University)

Acknowledgement

I am very grateful to everyone who has, in some way or another, helped me in the completion of my thesis on 'The Quest for the Most Suitable Density Profile of the Bubble Nuclei'.I am deeply grateful to my thesis advisor and mentor **Dr. Soumendu Jana** for his unwavering support, guidance and encouragement throughout this research journey. Without his constant mental and humane support, this work would not have been successful.

I wish to express my sincere thanks to **Dr Kulvir Singh**, Professor and Head, School of Physics and Materials Science, Thapar Institute of Engineering and Technology, Patiala, for providing me with all the necessary facilities for my research.

I also express my heartfelt gratitude to my lab mates and PHD scholars,**Mr Neeraj Sharma, Ms Gurpreet Kaur and Ms Anjali Saini**. Their discussions and camaraderie made the research process enjoyable and stimulating.

A special thanks to **Dr Manoj Sharma**, Professor, School of Physics and Material Science, Thapar Institute of Engineering and Technology, Patiala, for helping me refine my research and helping me to look at the problem from another perspective. His expertise in the field of Nuclear physics was also crucial in the completion of this thesis.

I owe my family and friends gratitude for their unconditional support, understanding, and encouragement throughout this challenging endeavour. Their unwavering belief in me has been a constant source of motivation.

Certificate

I hereby certify that the work which has been presented in this thesis titled "The Quest for the Most Suitable Density Profile of the Bubble Nuclei", submitted in partial fulfilment of the requirements for the award of the degree of Masters of Science in Physics at Thapar Institute of Engineering and Technology, Patiala, is an authentic record of my own work carried under the supervision of Dr Soumendu Jana, Professor, School of Physics and Material Science and refers other researcher's work which is duly listed in the reference section. The intellectual content of this thesis is the product of my own work and contains no material which, to a substantial extent, has been accepted for the award of any other degree at this or other educational Institution, except where due acknowledgement is made in the thesis.

Date:

(Purujeet Yadav)
Roll No. 302104001

This is to certify that the above statement made by the candidate is correct and true to the best of my knowledge.

DR. SOUMENDU JANA
Professor
School of Physics and Materials Science
TIET, Patiala

Certificate

I hereby certify that the work which has been presented in this thesis titled "The Quest for the Most Suitable Density Profile of the Bubble Nuclei", submitted in partial fulfilment of the requirements for the award of the degree of Masters of Science in Physics at Thapar Institute of Engineering and Technology, Patiala, is an authentic record of my own work carried under the supervision of Dr Soumendu Jana, Professor, School of Physics and Material Science and refers other researcher's work which is duly listed in the reference section. The intellectual content of this thesis is the product of my own work and contains no material which, to a substantial extent, has been accepted for the award of any other degree at this or other educational Institution, except where due acknowledgement is made in the thesis.

(Purujeet Yadav)
Roll No. 302104001

Date: 29/07/2023

This is to certify that the above statement made by the candidate is correct and true to the best of my knowledge.

DR. SOUMENDU JANA
Professor
School of Physics and Materials Science
TIET, Patiala

Contents

Abstract

In the centre of a bubble nucleus, the neutron and proton density is lower. Consequently, both the mass and charge density profiles exhibit a central depression. Complex and laborious numerical methods are utilised to disclose the profile of the bubble nucleus. Currently, numerous mathematical profiles feature a central decline. This thesis investigates the prospect of a correlation between mathematical profiles and the density profile of bubble nuclei. Considered are ten distinct categories of mathematical profiles. Bimodal skew-symmetric normal distribution emerged as the optimal profile, while Cosh-Gaussian performed well in instances where the bubble structure was more pronounced. A comprehensive and comparative report is provided.

1. CHAPTER 1
INTRODUCTION

1 Bubble nucleus and its importance

The secret to comprehending the fundamental properties of matter lies in the nucleus, a small but immensely dense core in the centre of an atom. It controls the complex dance of particles inside and is dense with protons and neutrons, acting as the centre of atomic stability. Scientists have been enthralled with the nucleus for decades, from its discovery and research to unravelling its structure and behaviour, leading to ground-breaking insights into the universe's fundamental elements. Within this deep realm of atomic nuclei lies a phenomenon that challenges our present knowledge of nuclear structure called 'bubble nucleus'. Unlike our traditional nuclei that have a constant charge and mass density, bubble nuclei possess a striking feature, a hollow or a bubble-like structure inside the core. This bubble-like structure is formed due to the paucity of protons and neutrons deep within the core of the nuclei.

Nuclear mass density and charge density are both measures of the distribution of nucleons(proton and neutron) inside the nucleus. Nuclear mass density refers to the distribution of the mass of the nucleus and is typically measured in units of mass per unit volume. It is usually determined by measuring how the nucleus scatters high-energy electrons or neutrons, and it can also be calculated theoretically using models such as the Hartree-Fock model or the Skyrme model.

Charge density refers to the distribution of electric charge inside a nucleus and is typically measured in units of charge per unit volume. It is related to the distribution of protons in the nucleus, which are the only charged particles in the nucleus. Charge density can be measured using techniques such as electron scattering, and it can also be calculated theoretically using models such as the Hartree-Fock model.

Both nuclear mass density and charge density are important in understanding the nucleus properties, such as the charge radius, binding energy, and electromagnetic properties. They

are also important for understanding the dynamics of nuclear reactions and the behaviour of nuclei in extreme conditions, such as those found in neutron stars or during heavy-ion collisions[1].

Usually, the charge and neutron density are assumed to be constant throughout the nucleus except at the boundaries. This constant density can be referred to as saturation density. This hypothesis is based on the assumption that the nucleons in the nucleus are closely packed together and repulsion between them is balanced by a strong attractive force called the strong force[1].

Fermi distribution is a statistical model that describes the distribution of nucleons inside the nucleus in terms of the Fermi energy, which is the energy at which the probability of finding a nucleon is half. The Fermi energy is determined by temperature, density and number of nucleons inside the given nucleus. The Fermi distribution is closely related to the constant nuclear density hypothesis[2, 3].

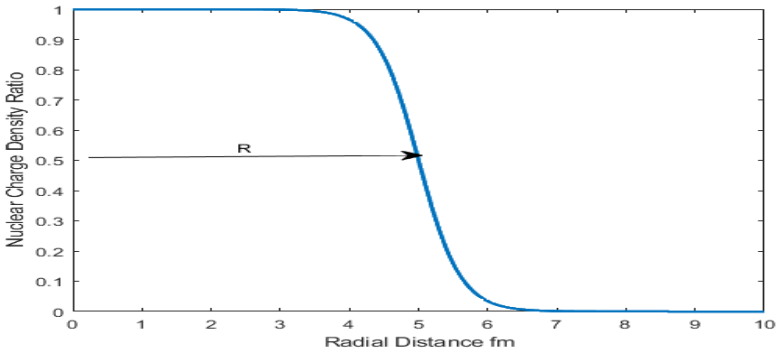

Figure 1: Ideal Charge Density Profile

But in the case of some nuclei, the charge density or the neutron density at a radial distance near the centre of mass of the nucleus is found to be higher or lower than the given constant value. This phenomenon of central depletion of charge due to paucity of proton and neutron is called a bubble nucleus.

The phenomenon of bubble nuclei was found when studying the charge density and neutron density profile of various nuclei[4, 5]. The idea of bubble nuclei was first proposed in 1950 as a theoretical possibility to explain isotopic shifts in certain nuclei. However, since then, experimental data have ruled it out and it is not observed in nature. Despite the fact that

bubble nuclei do not exist in nature, the study of such nuclei is still of theoretical interest. The study of bubble nuclei can help to understand the properties of nuclei under extreme conditions, such as those found in neutron stars or during nuclear reactions. Additionally, the study of bubble nuclei can also test the limits of current nuclear models and guide the development of new models that better describe the behaviour of nuclei.

Several causes of this phenomenon have been proposed. For lighter nuclei, it may be due to proton or neutron in-occupancy in the s-state, which lies near the Fermi energy level. This causes the central density of the nucleus to either become notably lower than the saturation density or vanish[6, 7]. In some cases, the inner s orbital is depopulated caused by inversion of $s_{1/2}$ with any other state located above (usually a d,h and f state). For example inversion of $2s_{1/2}$ and $1d_{3/2}$ or $3s_{1/2}$ and $1h_{11/2}$[8]. While, for heavy and super heavy nuclei, the bubble phenomenon is caused due to coulombic repulsion or rather, it's the result of a dynamic interplay of the Coulomb and nucleon-nucleon forces[9, 10, 11, 12]. However, hindrance in the formation of the bubble structure can be attributed to deformation in the nucleus and to the pairing correlation effects. Interestingly the bubble phenomenon occurs in a wide range of atomic mass.[13, 14].

Depletion fraction (DF) is usually used to quantify the occurrence of bubble structure in a certain nucleus and is defined as

$$DF = (\rho_{max} - \rho_c)/\rho_{max}$$

where $\rho_c = \rho(r = 0)$ and ρ_{max} represent the value of central and maximum charge density respectively. The depletion factor depends highly on the quantal effects which is related to the filling of single-particle levels near Fermi Energy. One might be curious as to why only the s orbital is considered when talking about the bubble nucleus. The straightforward explanation is that only for the s-orbital is the wave function non-zero at the origin (r=0), with the radial distribution peaking at the nucleus centre. The non-zero l orbitals which are suppressed deep inside the nucleus have no contribution to the central nuclear density. Therefore the best possible candidates to study the bubble structure phenomenon are those which have unoccupied s-orbitals. This is a necessary condition for the bubble effect, but

additionally, the s-orbital close to the fermi energy must be surrounded by orbitals of larger l (the larger, the better), which should be separated in energy from its nearby single-particle states so that dynamical correlations are feeble. In addition, it is essential to observe that the depletion in the centre caused by the vacancy in the s-orbital is exacerbated by the occupied orbitals whose maximum occurs at great distances. Therefore, the combination of both conditions could potentially maximise the bubble effect. Various studies have been carried out to study the bubble structure and anti-bubble effect at high temperatures[15]. The existence of bubble nuclei has also been studied in magic nuclei[16].

It was observed that 30Ne, 32Mg and 34Si (Z=10,12 and 14) in N = 20 isotones and 22Si(Z=14) in N = 8 isotones, show strong bubble structure and show a prominent central depletion. The isotones 46Ar, 56S, and 58Ar with N=28 and 40, as well as the isotones with N=126 and Z = 48-78, exhibit significant central depletion and are therefore marked as suitable candidates for bubble formation. But isotones with N=50 and 82 show no central depression indicating that they do not form the bubble structure. The simple reason being that they have no s-orbital near the Fermi level(see Figure 2 from [16]).

Unoccupancy of $s_{1/2}$ state in the isotopes of O(N=8-14), Ca(N=14), Ni(N=40-52), Zr(N=40-60), Sn(N=48-60) and Pb(N=126-158) is indicative of central density depletion formation as shown in their respective neutron density plot(Figure 4 from [16]). Although the Fermi level in Ni and Zr is far from the unoccupied 3s state, it appears to influence central depletion formation still. It was also observed that the 2s state demonstrates a greater density depletion than the 3s and 4s states.

Research has also been done to study 34Si and 22O as possible proton and neutron bubble nuclei using 3 theoretical frameworks(shell model, relativistic and non-relativistic microscopic mean field theory). The research concluded with an overall agreement of proton bubble nuclei being present in 34Si nuclei in all frameworks, while the phenomenon was framework dependent in the case of 22O.[17]

Anti-bubble effect due to high temperature and deformation in light, medium heavy and super-heavy nuclei was also studied. It was determined that the s-orbital surrounded by a larger l orbital and separated in energy from adjacent s, p states to ensure weak dynamical correlation produces the greatest bubble effect. The effect of shell structure on bubble nu-

clei has thus far only been reported for nuclei below 208Pb. It has been observed that the coupling correlation and dynamical quadrupole shape effect hinder the bubble effect but are unable to eliminate it. However, there appears to be an anti-bubble effect at a certain temperature threshold. Also studied is the effect of temperature on the occupancy of s-orbital, which indicates the possible function of temperature in central depletion.[18].

2 Different Models to Study Bubble Nucleus Profile

Several theoretical models have been used to study bubble nuclei and predict their various properties and behaviour under various conditions. Some of these theoretical models are the Hartree-Fock model, liquid drop model, shell model, and relativistic mean field (RMF) model.

2.1 Liquid Drop Model

Liquid drop model has been one of the most widely used models to study all types of nuclei. In this model, the nucleus can be described as a semi-classical fluid consisting of protons and neutrons, inside which exists an internal repulsive electrostatic force that is directly proportional to the number of protons. These particles are considered to be quantum particles that follow the Pauli exclusion principle, which states that two nucleons of the same kind can not occupy the same state. This fluid is also called a Fermi liquid. The density is taken to be constant pertaining to various scattering studies. The nucleus is assumed to be spherical in shape. This spherical nucleus can be twisted in a dumbbell shape and broken, given enough energy. This model is still used as it provides accurate binding energy for most of the nuclei[1].

2.2 Shell Model

The binding energy of certain nuclei seems to show systematic deviation from what is found using the liquid drop model. These nuclei have a certain number of protons and neutrons and

are more tightly bound than their neighbouring nuclei. These nuclei can be classified as singly or doubly magic. These observations lead to the inception of the shell model. According to this model, the nucleons seem to occupy certain discrete energy levels. These levels are not uniformly distributed. States occupying certain intervals of energy are crowded, while some are empty, which generates a gap in possible energies. A shell is a set of energy levels separated by a large gap. The energy levels in this model are found by solving the Schrödinger equation for a single nucleon which moves through an average potential generated by all other nucleons. Each level is either occupied or empty. When several quantum states pertain to a single energy value, these states are said to be degenerate. Degeneracy is prominent if the average nucleus has some symmetry. This idea of the shell helps to explain why some nuclei are more stable than others. Using the Pauli exclusion principle, the nucleon of the same kind can not occupy the same energy state. So the nucleus's ground state is where the shells are filled from the lowest to some level. A Nucleus with a full shell is extremely stable.

2.3 Relativistic Mean Field Theory

The relativistic mean field theory (RMF) model is one of the most successful and extensively used theoretical approaches to study finite nuclei as well as infinite nuclear matter and neutron stars. In the RMF theory, it is assumed that the nucleons oscillate independently, just like a harmonic oscillator in a mean-field produced via an exchange of photons and mesons. RMF theory, consist of several force parameters set like L1, L2, SH, NL1, NL2, NL3, NL3*, G1 and G2 for linear and non-linear lagrangian. It is widely accepted that the NL3 parameters reproduce the nuclear saturation properties the best compared to other parameters throughout the periodic table. NL3* parameter set is an improved version of NL3, which is extensively used for all nuclei to reproduce the experimental binding energy and other physical observables[19, 20].

This work uses the Spherical Relativistic mean field(sph RMF) and definite Relativistic Mean Field(def RMF). In this approach, the potential is assumed to have a central component that depends only on the radial component. By assuming spherical symmetry, the calculation becomes more efficient but limits itself to a spherical shape and cannot describe deformed nuclei. In contrast, the def-RMF approach can be applied to all deformed nuclei, where the

nuclear mean field is not spherically symmetric. This becomes important when studying exotic or heavy nuclei which are generally non-spherical in shape due to shell structure and collective excitation.

2.4 Hartree Fock Method

The Hartree-Fock method is a theoretical approach used to approximate the behaviours of many-body quantum systems. Hartree-Fock Mean Field is a non-relativistic mean-field approach that is dependent on the choice of the appropriate effective interaction potential.

In our case, Skyrme Hartree Fock Method is used. It is a zero-range interaction. It assumes the nucleus as a system of interacting nucleons and the nucleon-nucleon interaction is approximated by a Skyrme force. It is a 2 body interaction that takes into account the central and spin-orbit components of the nuclear interaction. Within the Hartree-Fock approximation, each nucleon is assumed to move independently in a mean-field created by other nucleons[21].

3 Motivation

The profile of the bubble nucleus is obviously a bell-shaped one with usually a central dip or almost flat top in some cases. So it is a common scientific curiosity to correlate the bell-shaped (or near bell shaped) mathematical profiles, e.g., Cosh-Gaussian, Bimodal Skew Symmetric Normal distribution, Normal Distribution, Laplace distribution, Cauchy Distribution, Modified Bessel Function, Ricker Wavelet, Raised Cosine function and Gompertz Curve etc. with the charge density and neutron density profile of the bubble nuclei. In this thesis, we check this closeness/proximity/resemblance of the mathematical functions with the charge distribution and select the best one or few. This is a small step towards quantifying the bubble structure using a mathematical model. To the best of our knowledge, no known attempt has been done to describe the bubble nucleus profile using the bell shaped profiles. Therefore we propose to correlate the popular bell-shaped (or near bell-shaped) mathematical profiles with the density profile of the bubble nuclei. More, precisely, to correlate the nuclear parameters with the parameters of the bell-shaped profiles.

4 Objectives

The main objectives of our investigation are :

- To identify the mathematical profile that produces the closest fit to the bubble nucleus profile.
- Categorizing mathematical profiles as per the degree of matching with bubble nucleus.

5 Methodology

To achieve the above-mentioned objectives, the following methodology has been adopted. The course of action taken during the completion of the investigation is mentioned here step by step. Only those nuclei were chosen, which showed prominent bubble structures in their charge density and neutron density profile with radial distance. The experimental data used only three frameworks to evaluate the charge density vs radial distance plots. These are spherical relativistic mean field theory, definite mean field theory and Hartree-Fock theory. Only 22O, 23F, 34Si, 36S, 36Ar and 46Ar showed promising results under this framework. The plots of charge density vs radial distance and neutron density vs radial distance evaluated using the framework mentioned above for these nuclei were referred to.

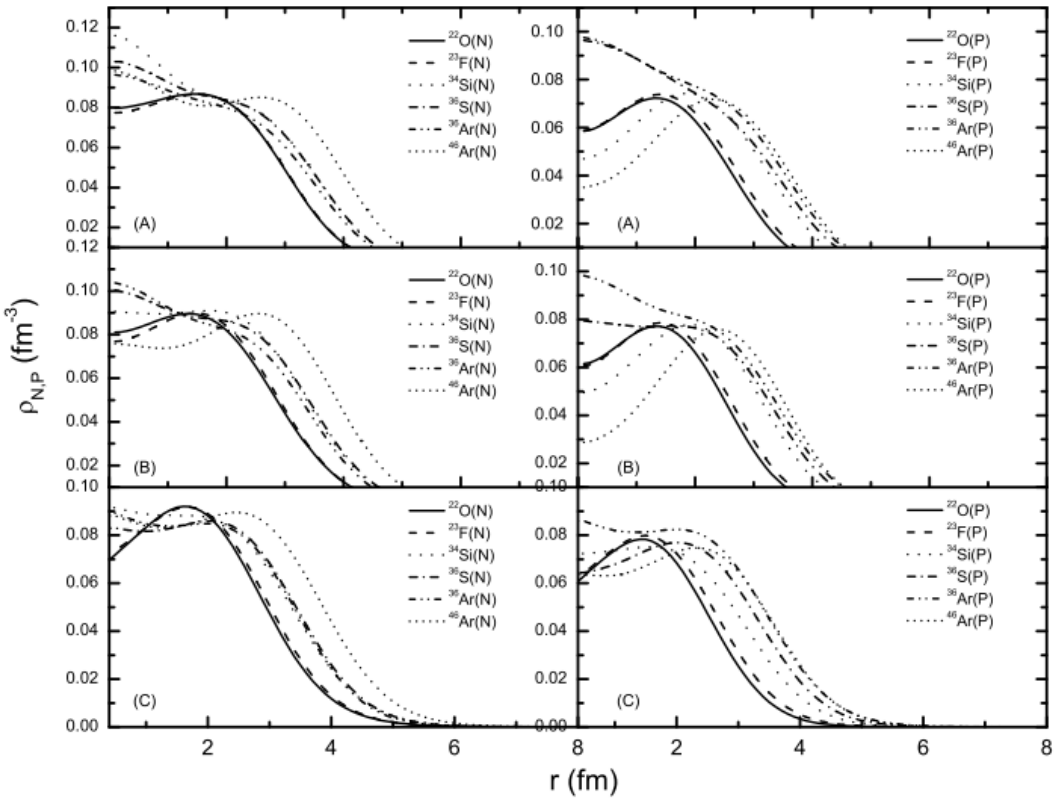

Figure 2: A typical source of extraction of primary data that has been used as input
Image Courtesy: Sharma, M.K., Panda, R.N., Sharma, M.K. and Patra, S.K., 2015. Nuclear structure study of some bubble nuclei in the light mass region using mean field formalism. Chinese Physics C, 39(6), p.064102.

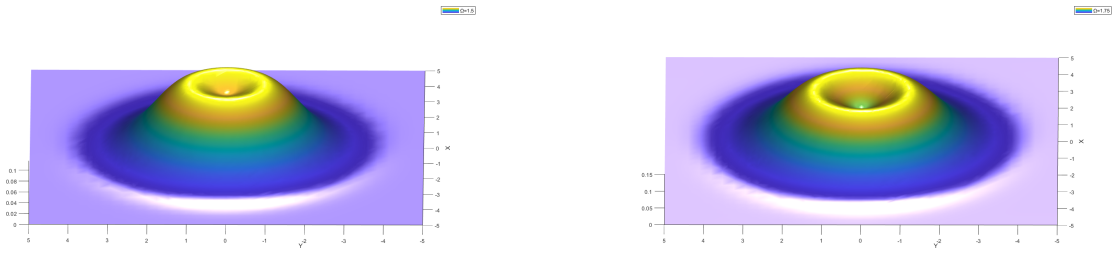

Figure 3: 3-dimensional plots of 2 Cosh-Gaussian curve having different value of A_0 and a which show a prominent dip at the centre

Due to the unavailability of experimental data points, the data points for charge density versus radial distance and neutron density versus radial density were obtained using an online plotter named 'WebPlotDigitizer'. The charge density and neutron density plots were uploaded, and the coordinates for a given nucleus in a given framework were recorded in an

Excel file. Calibrating the axis and manually pressing and capturing these data points were necessary. Manual error risks could not be eliminated, but the plots were to be reproduced using a Cosh-Gaussian profile. The collected data point possessed the fundamental curvature of the graphs and can be used to evaluate the procedure. The given input plot as shown in Figure 3 contains the charge density profile vs radial distance plots calculated using the frameworks: The definite relativistic mean field model, the spherical relativistic mean field model and the Hartree-Fock model. All the plots on the left are for neutron charge density, and the plots on the right are for proton charge density. A, B and C tags under the plots denote the framework used. A is for HF, B for sph. RMF, C for def. RMF.

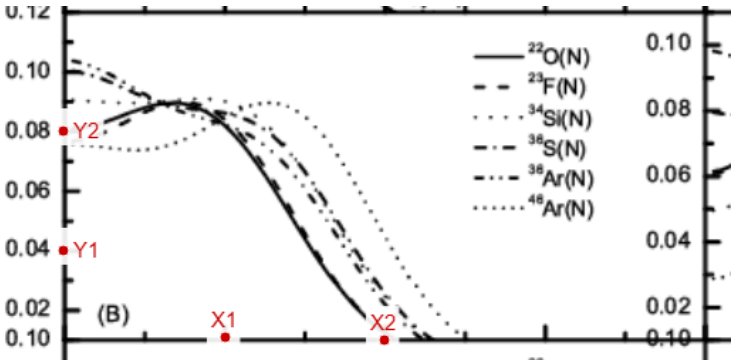

Figure 4: Calibration of the axis on "WebPlotDigitizer"

Figure 4 shows the calibration process in which $X1$, $X2$, $Y1$ and $Y2$ points are the calibration points. $X1$ and $X2$ points are used to calibrate the X-axis. Similarly, $Y1$ and $Y2$ points are used for Y-axis calibration. The X-axis denotes the radial distance in the fermi-meter and the Y-axis denotes the radial charge density $\rho_{N,P}$ fm^{-3}. For the given figure value of $X1$, $X2$, $Y1$ and $Y2$ was set to 2, 4, 0.04 and 0.08 respectively.

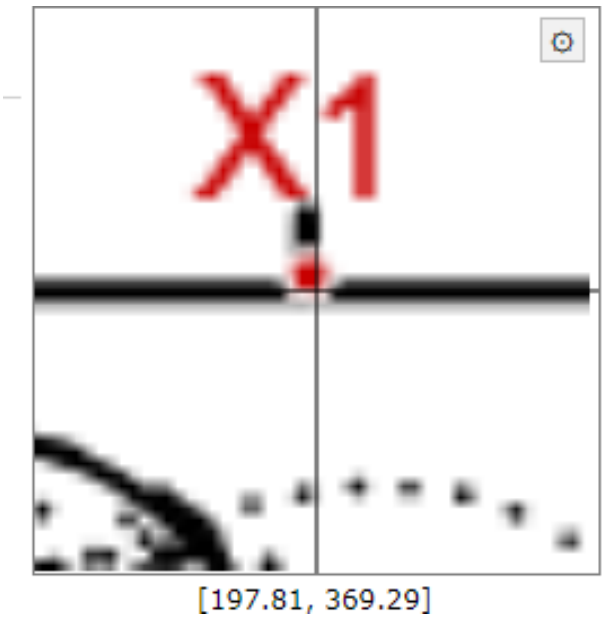

Figure 5: Zoomed-In picture when selecting the calibration point

Zoomed-in picture of the plot was also available when selecting the calibration points as well as data points.

After the calibration process was complete data points for each nuclei for the 3 frameworks had to be collected. At least 30 points were taken for each nucleus.

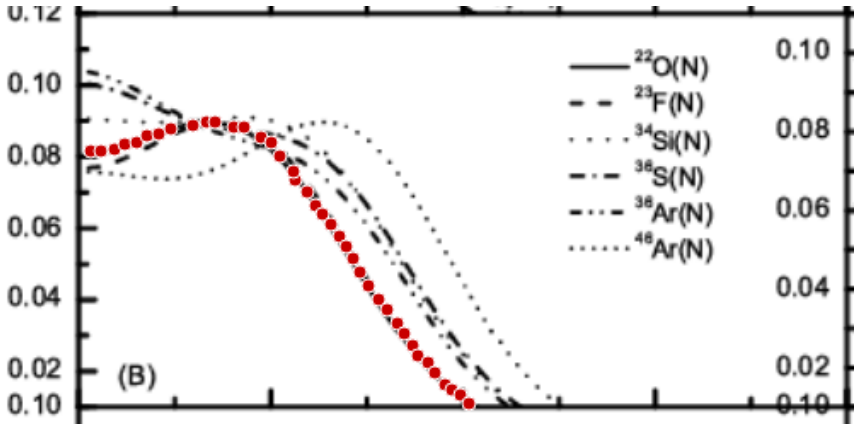

Figure 6: Collection of neutron density vs radial distance data points for 22O

These data points were collected and then used in Matlab to reproduce the same plot on it and compare it with various mathematical models we used. In the case of Cosh-Gaussian, the profile used was in the form of

$$A_0 \cosh(\Omega.r/a) \exp(-r^2/2a^2)$$

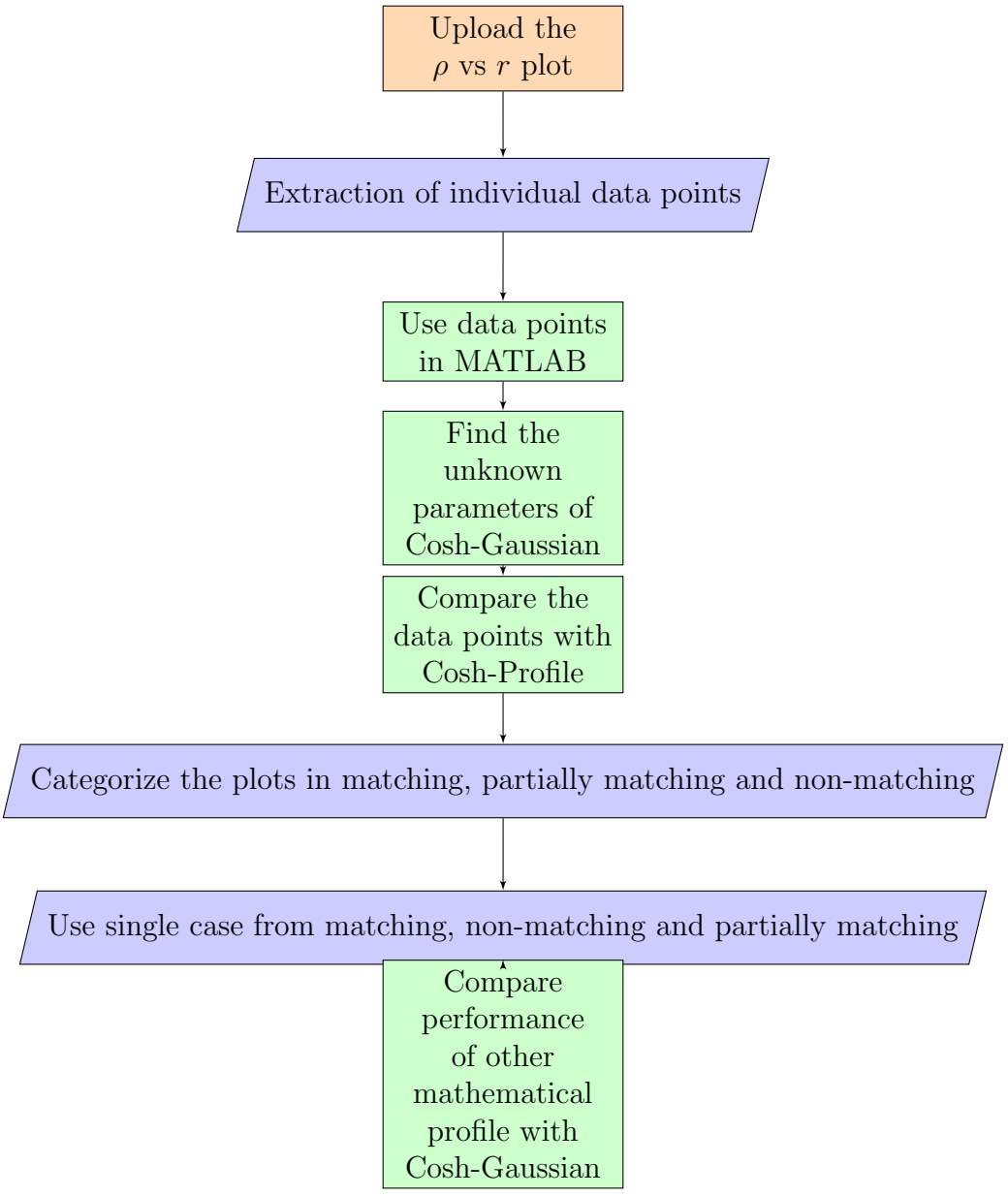

Figure 7: Illustration of the procedure followed during the research work

Our aim was to find the various parameter required (in the case of the Cosh-Gaussian curve:Ω, a, and A_0) values that match the data points collected. The data point collected

had charge or neutron density value for a corresponding radial distance r. A function was made in Matlab to calculate the norm of the difference between the charge density data point value and the Cosh-Gaussian profile value at the respective r value. This function was called in the main program and the respective value of the parameters (in case of Cosh-Gaussian: Ω, A_0, and a) were found for which the norm of the difference in minimum using fminsearch function. 'fminsearch' is a predefined method that uses the derivative-free method to minimize an unconstrained multi-variable function . 'fminsearch' uses the Nelder-Mead simplex algorithm. The Nelder–Mead method (also known as the amoeba method, downhill simplex method or the polytope method) is a numerical method used to extract the maxima or the minima of an objective function in a multidimensional space. It is a direct search method (based on function comparison) and is often used in nonlinear optimization problems for unknown derivatives.

The results obtained were compared to results evaluated by another Matlab's inbuilt function called 'fmincon'. 'fmincon' uses the interior-point method. Interior-point methods (also referred to as barrier methods or IPMs) are a certain class of algorithms that are used to solve linear and nonlinear convex optimization problems. These functions basically are used for minimization problems where the unknown parameter are multiple. The only drawback of using these methods is they require a random starting point for minimization. Prior knowledge of the range in which the results may be present is beneficial. These methods usually are not able to find a global minimum and hence are used in conjugation with Globalsearch function to refine their search process. As we had no prior knowledge of any constraints regarding the function we used, these methods were the only viable option.

2. CHAPTER 2
FUNDAMENTALS OF VARIOUS MATHEMATICAL PROFILES

In this chapter, we discuss the various mathematical profiles that have a central dip and primarily resemble the profile of bubble nucleus charge density.

1 Cosh Gaussian Details

The shape of the proton charge density and neutron density in these nuclei apparently matches the Cosh-Gaussian(CHG) profile under certain circumstances. The Cosh-Gaussian profile basically is defined as a product of a cos-hyperbolic function with a Gaussian function. Its mathematical form is

$$Y = A \ \cosh(\Omega x) \exp(-x^2/a^2)$$

where the exponential term is the Gaussian and Ω is a parameter associated with the cosh part. A_0 is a constant parameter and a is the parameter associated with a half-width at $1/e$ intensity point for the Cosh-Gaussian beam. Expanding the cosh term in the above equation as a sum of exponential we get

$$Y = \frac{A_0}{2}(\exp(\Omega.r) + \exp(-\Omega.r)) \exp(r^2/2a^2)$$

which after simple mathematical manipulations gives

$$Y = \frac{A_0}{2} \exp \frac{\Omega_0^2}{2}(\exp \frac{-1}{2}(\Omega_0 - \frac{r}{a})^2 + \exp \frac{-1}{2}(\Omega_0 + \frac{r}{a})^2)$$

where $\Omega_0 = \Omega a$. The above equation signifies that the Cosh-Gaussian beam can be produced by the superposition of 2 decentered Gaussian beams whose centres are located at $\Omega_0 = r/a$ and $\Omega_0 = -r/a$ respectively

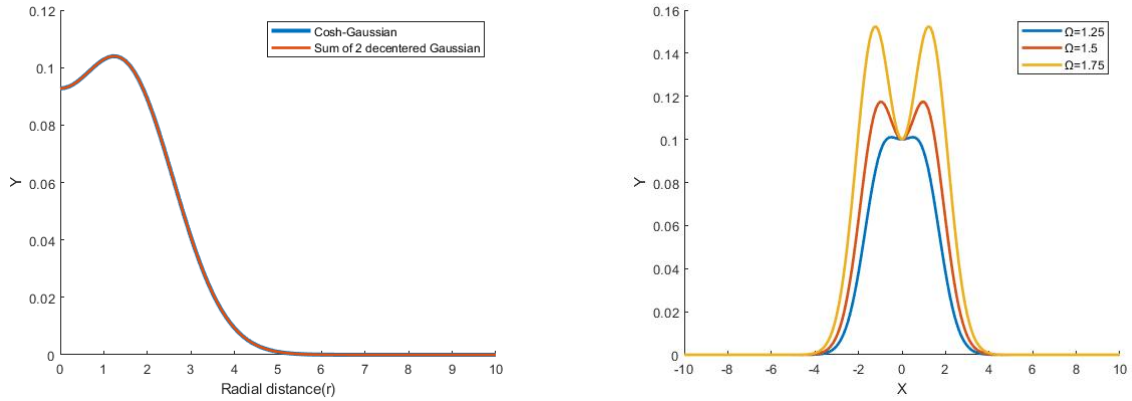

Figure 8: The figure on the left shows that a Cosh-Gaussian beam is a sum of 2 decentered Gaussian beams and the one on the right shows the variation in the Cosh-Gaussian profile with Ω

The shape of the proton charge density and neutron density in these nuclei apparently matches the Cosh-Gaussian profile under certain circumstances. The Cosh-Gaussian profile finds utility in many areas of physics and communication. Mostly propagation of the Cosh-Gaussian beams through various environments is studied. It has been found that 2 decentered Gaussian beams can be used to produce a Cosh-Gaussian beam and its propagation expression obtained.

Propagation of the Cosh-Gaussian beam in plasma having density ripples has also been studied. Consideration has been given to the effect of the change in refractive index caused by relativistic laser-plasma interaction and pondermotive force on the self-focusing of the laser beam.[22]. Here a pondermotive force is a non-linear force experienced by a charged particle in an oscillating in-homogeneous electromagnetic field. How the periodic density ripple effect the self-focusing of laser at different intensities and wavelengths of the laser as also been studied[23].

Analytical vectorial structure of the CHG beam has been studied in the far field. Moreover its light intensity distribution,i.e. its TE and TM mode investigated. The analytical formula found is applicable to both par-axial as well as non-par-axial cases[24]. For some special cases, the CHG beam reduces to a Gaussian beam. Non-linear absorption of CHG beams on second harmonic generation in colloidal plasma has also been investigated. It was found that

the non-linear absorption decreases with increases in decentered parameters[25]. Analysis of propagation of CHG beams in plasma without temperature gradient and with exponential temperature gradient was done[26].

Other than CHG propagation in plasma its behaviour in turbulent atmospheres is also of keen interest to many. For example, a paper in 2011 studied the asymptotic on-axis behaviour of a CHG beam in a strong turbulent atmosphere[27]. Some leading papers also found that a Cos-Gaussian beam is transformed into a Cosh-Gaussian beam after it undergoes natural diffraction[28]. Propagation of CHG beams in a strong turbulent environment through an ABCD optical system is also a leading topic in research[29]. The ABCD optical system is a mathematical model for describing the propagation of paraxial rays within an optical system. In geometrical optics, it is commonly employed to analyse and design optical systems such as lenses, mirrors, and narrow lenses. Important parameters, including image distance, magnification, and image quality, can be calculated using the ABCD matrix formalism after which the analytical expression for average intensity at the receiver plane is studied.

In a turbulent environment, the propagation of higher-order CHG beams through a paraxial and real ABCD optical system has been studied. For smaller beam parameters and a larger structure constant, the Cosh-Gaussian beam of higher order disperses more quickly in a turbulent atmosphere.[30]. In addition, an analytical formula for the average intensity of Cosh-Gaussian (CHG) beams diffracted by an aperture in a tumultuous atmosphere has been developed, and its limiting cases have been discussed. It was found that the evolution properties of the average normalised intensity profile in a turbulent atmosphere with an aperture differ not only from those of free space with an aperture, but also from those of a turbulent atmosphere without an aperture.[31].

2 Ricker Wavelet or Mexican hat wavelet

Ricker wavelet also known as the Mexican hat wavelet is defined as a re-scaled/normalized negative second derivative of a Gaussian curve. It is a part of Hermitian Wavelets which are special cases of continuous wavelets. It finds its utility in modelling seismic data and as a source term in computational electrodynamics. Its mathematical form is as follows:

$$Y = A_0(1 - x^2) \exp \frac{-x^2}{2}$$

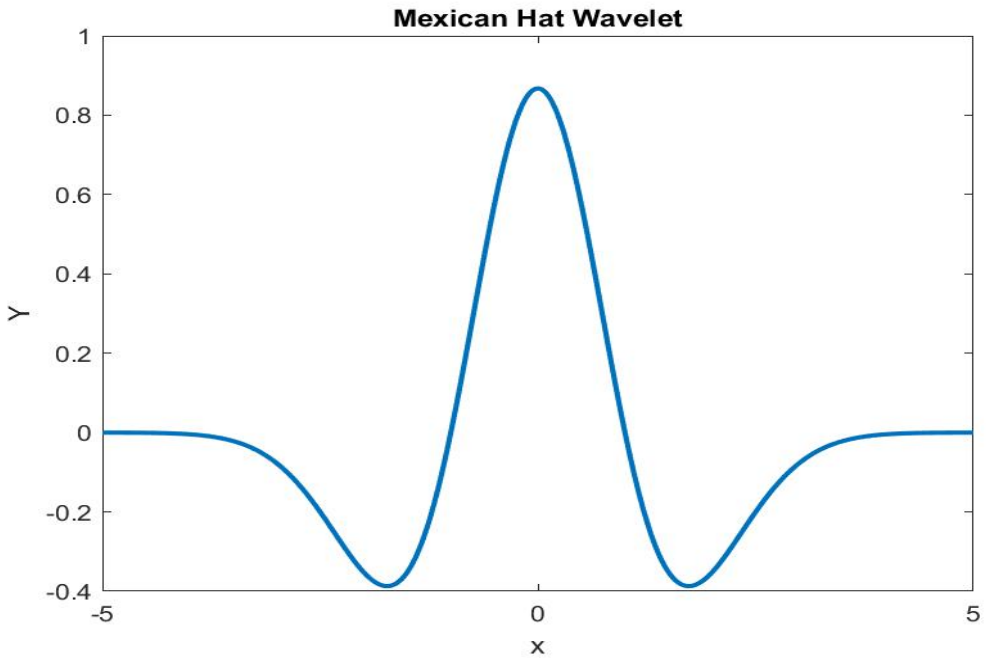

Figure 9: General plot of Mexican Hat wavelet or a Ricker Wavelet

3 Cauchy Distribution

Cauchy distribution more commonly known as the Lorentz distribution is a continuous probability distribution. It can also be defined as the ratio of 2 normal distributions of random variables with zero mean. They are usually used to define a pathological distribution because of it having undefined expected value and variance. Only fractional moments less than one exist for a Cauchy distribution. It is a stable probability distribution and can also be expressed analytically.

The probability density function of the Cauchy Distribution is defined as :

$$Y = \frac{1}{\pi} \frac{\gamma}{(x - x_0)^2 + \gamma^2}$$

where x_0 defines the peak of the distribution and γ defines the half width half maxima. γ is sometimes also called a probable error.

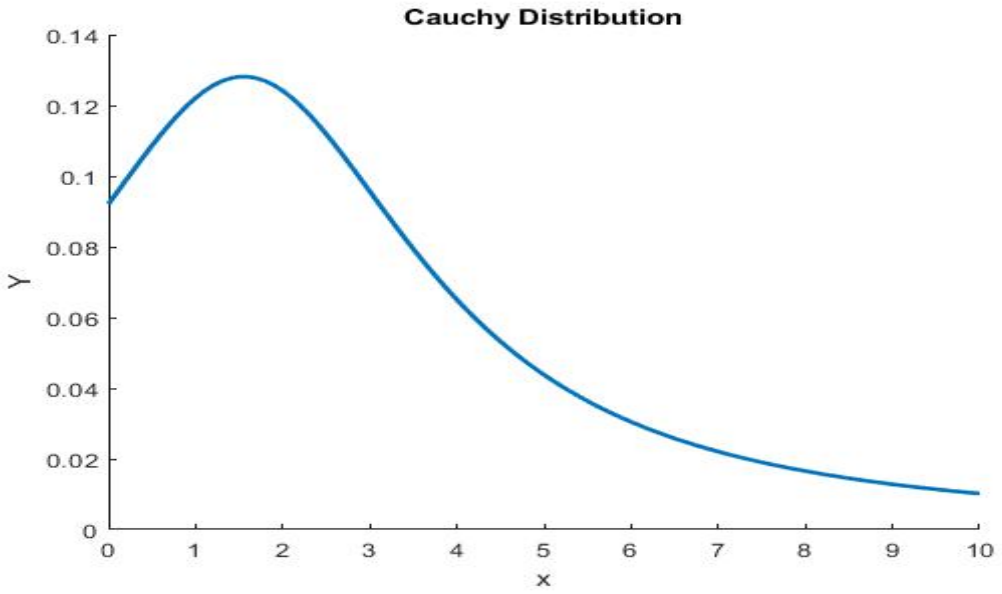

Figure 10: General plot of a Cauchy distribution

4 Laplace Distribution

The Laplace distribution is also part of a continuous probability distribution. Because of its resemblance to 2 exponential distributions sliced together along the abscissa, it is also called the double exponential distribution. It is defined as the difference between 2 independent random variables which have an identical exponential distribution. It finds its utility in modelling data with heavy tails or one having a higher peak than a normal distribution. Its probability density function is defined as :

$$Y = \frac{1}{2\ b}\ \exp\frac{-|x-\mu|}{b}$$

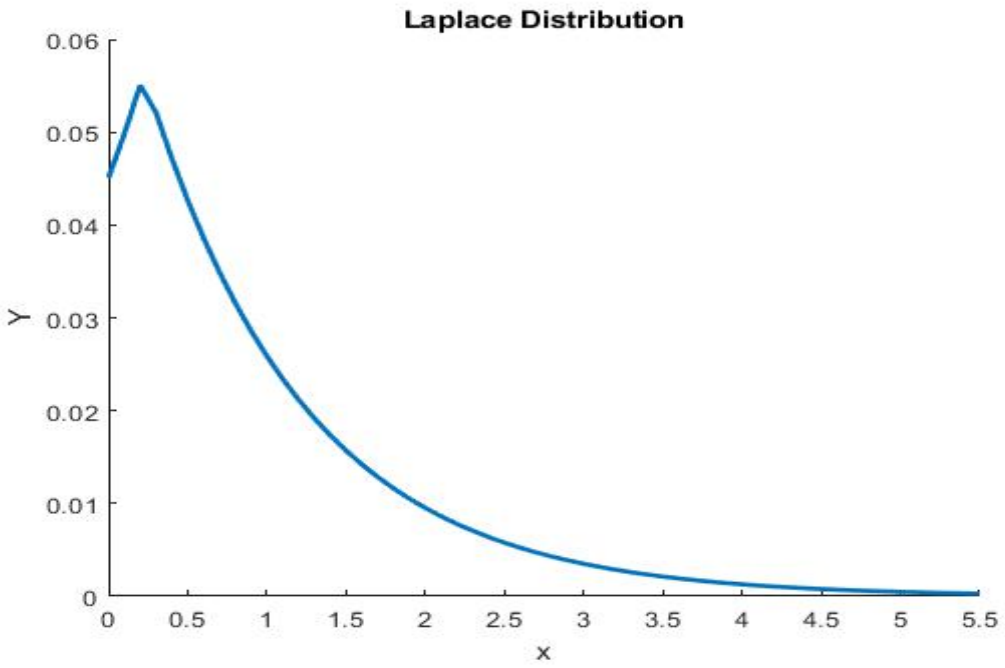

Figure 11: General plot of a Laplace distribution

5 Raised Cosine Function

Raised cosine function, an implementation of low pass Nyquist filter is a function used to shape the pulse in transmission systems. The cosine function is the non-zero portion of the frequency spectrum of its simplest form (β =1) , which is 'raised' up to sit above the f (horizontal) axis and hence its name is the raised cosine function Its frequency response $H(f)$ is symmetric at about 0 Hz. It is divided into 3 parts:

- A flat or constant part inside the pass-end
- A cosine curve that sinks to zero in the transition region
- 0 outside the pass-end

Its frequency response $H(f)$ is defined as:

$$H(f) = \begin{cases} 1, & |f| \leq \frac{1-\beta}{2T} \\ \frac{1}{2}[1 + cos(\frac{\pi T}{\beta}[|f| - \frac{1-\beta}{2T}])], & \frac{1-\beta}{2T} < |f| \leq \frac{1+\beta}{2T} \\ 0, & \text{otherwise} \end{cases}$$

where β is the roll-off factor and T is the symbol period of communication systems. The value of β is between 0 and 1. Raised Cos filter's ability to minimize intersymbol interference(ISI) helps in pulse shaping in digital modulation.

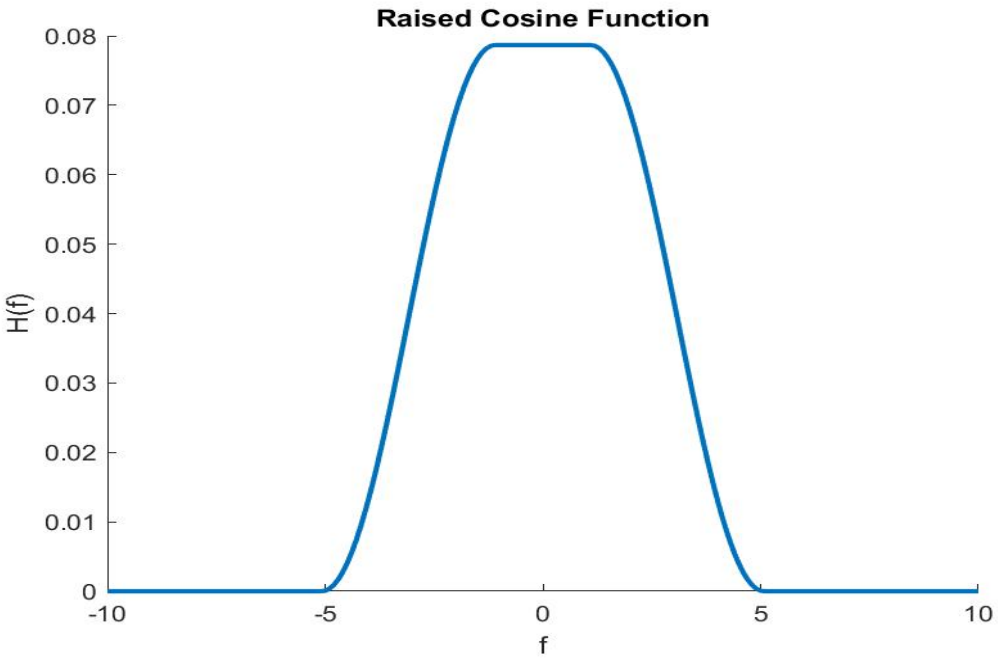

Figure 12: General Plot of a Raised Cosine filter or function

6 Normal Distribution

The normal distribution, also known as the Gaussian distribution, is the most used distribution in statistics and probability theory. It is also part of a continuous probability distribution. Most real-valued random variables can be nearly or completely described by the normal distribution. Its probability density function is defined as :

$$Y = \frac{1}{\sigma\sqrt{2\pi}} \exp -\frac{1}{2}(\frac{x-\mu}{\sigma})^2$$

Here the parameter μ is the mean or expectation value of the distribution while σ is the standard deviation. Its variance is defined as σ^2.

Its simplest case also called unit normal distribution is when $\sigma = 1$ and $\mu = 0$. The normal distribution is also the only distribution whose cumulants other than mean and variance are 0.

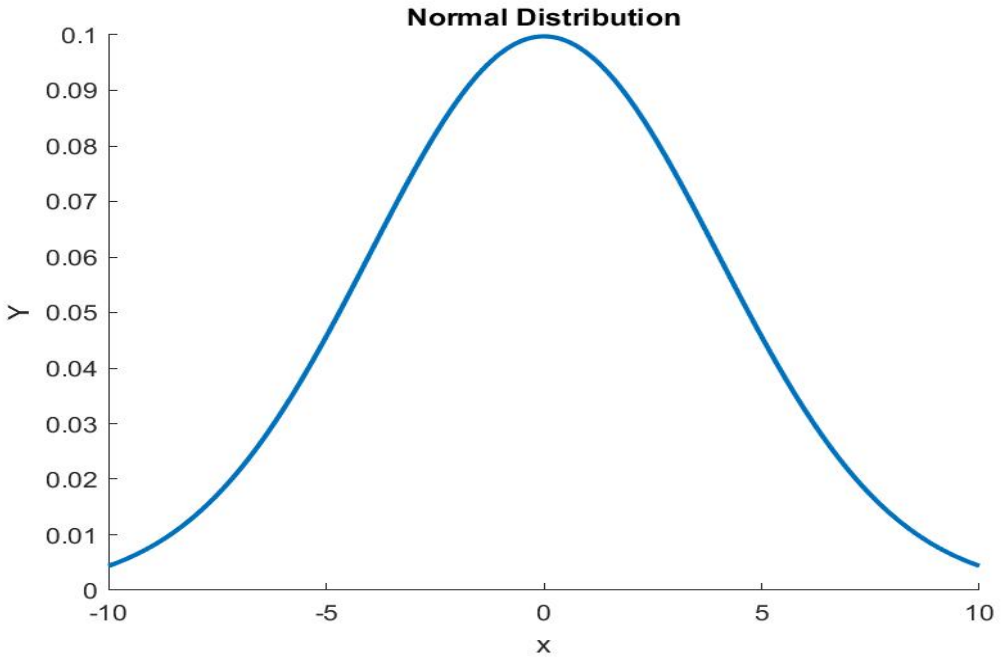

Figure 13: General plot of normal distribution

7 Gompertz Function

It is a mathematical model for time series and is a sigmoid function. It describes growth to be slowest at the start and end of a given time period. It is very similar to a logistic curve but for a smaller value of time, it grows at a faster rate than the logistic model curves. The future value of the function is approached at a larger rate than the lower-valued asymptote. It is defined as:

$$Y = ae^{(-be^{-ct})}$$

where a is the asymptote,b is the displacement along the x-axis, and c is the growth rate. It has a wide range of applications, from modelling of growth of tumours in humans to modelling the population in a confined space. It can also be used to examine disease spread in a region or model market impact in finance.

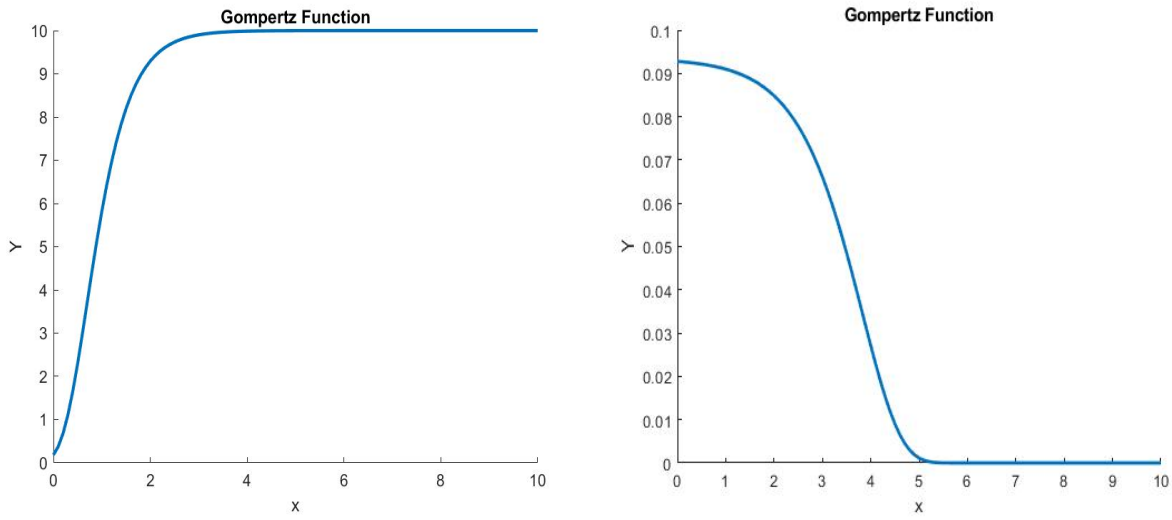

Figure 14: General Plots of Gompertz Curve

8 Modified Bessel's function of the second kind

Modified Bessel's function of the second kind is one of the solutions of Modified Bessel's differential equation. Also called the Basset function, it is an important function with applications in physics and mathematics[32]. It has also become important in fields like statistics and economics. The modified Bessel's differential equation is

$$x^2\frac{d^2y}{dx^2} + x\frac{dy}{dx} - (x^2 + v^2)y = 0$$

The solution of this differential equation is of the form:

$$y = AJ_v(ix) + BY_v(ix) \quad x > 0$$

or

$$y = CI_v(x) + DK_v(x) \quad x > 0$$

where $I_v(x)$ and $K_v(x)$ are the modified Bessel's function of the first and second kind respectively.

Unlike Bessel's function which is oscillating in nature, $I_v(x)$ and $K_v(x)$ grow and decay exponentially. For real values of v and $x > 0$ the Bessel's function of the second kind can be expressed as an integral of form

$$K_v(x) = \int_0^\infty f_{v,x}(t)dt$$

where

$$f_{v,x}(t) = cosh(vt)\ exp(-xcosh(t))$$

We have used the function $f_{v,x}$ which can be said to be the time derivative of the Modified Bessel's function of the second kind.

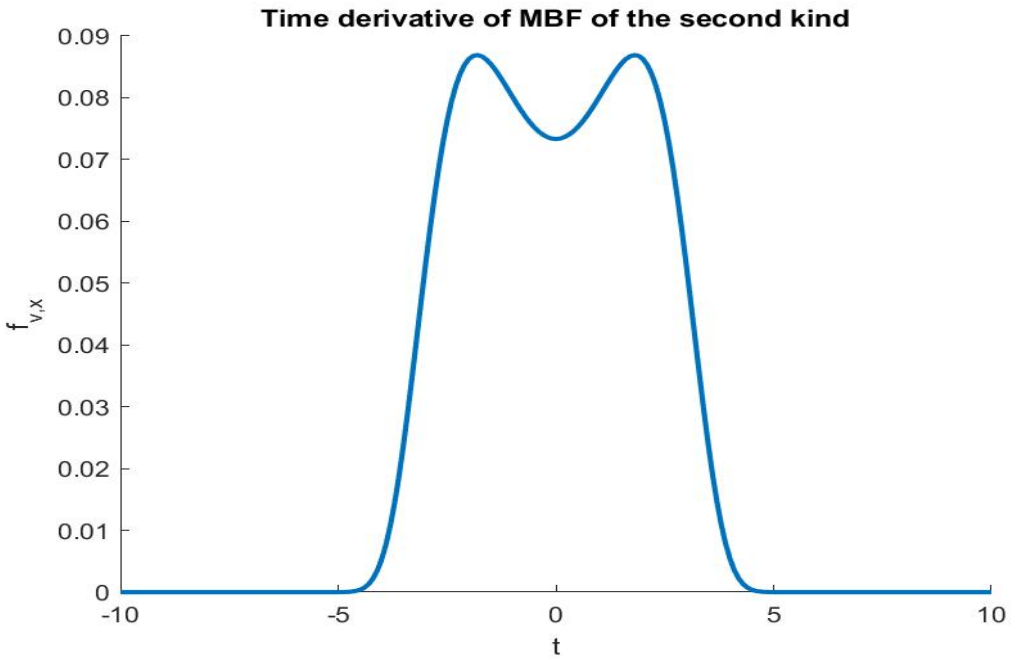

Figure 15: Plot of time derivative of Modified Bessel Function of second king

9 Conway-Maxwell-Poisson Distribution

Conway-Maxwell-Poisson distribution is a discrete probability distribution that generalizes Poisson's Distribution where an additional parameter is added to represent under and over dispersion. It is part of the exponential family. Its special cases are the Poisson and geometric distribution and its limiting case is the Bernoulli distribution. Its probability mass function is

$$P(x) = \frac{\lambda^x}{(x!)^\nu} \frac{1}{Z(\lambda, \nu)}$$

where $Z(\lambda, \nu)$ serves as the normalization constant. The parameter ν is an addition to Poisson's distribution and accounts for the decay rate adjustment. When ν is 1, the distribution becomes Poisson's distribution and when $\nu \to \infty$, the distribution approaches Bernoulli distribution.

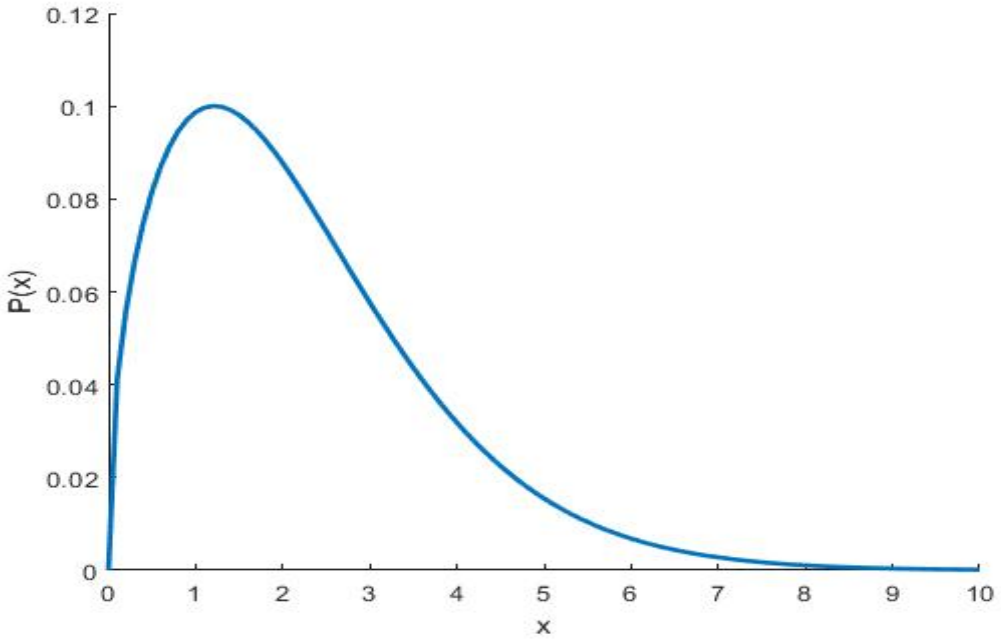

Figure 16: A general plot of Conway-Maxwell Distribution

10 Bimodal Skew-Symmetric Normal Distribution

Bimodal Skew-Symmetric Normal Distribution(BSSN) is the generalization of bimodal normal distribution. It is able to catch/capture the asymmetric and platykurtic/leptokurtic data sets. It is also able to capture different types of bimodality. Data-set from various fields which has bimodality, asymmetric and negative and positive kurtosis can be easily represented by the bimodal skew-symmetric normal distribution[33]. Its mathematical form is :

$$\Phi(x) = \frac{2\psi^{3/2}}{\gamma\sqrt{pi}}[\delta + (x-\beta)^2]\exp\left(-\psi(x-\mu)^2\right)$$

Here μ and β are the location parameters, whereas ψ and δ are the scale and bimodality parameters respectively.

BSSN distribution is seen as a viable replacement for a mixture of 2 normal distributions in cases where bimodality is of utmost importance.

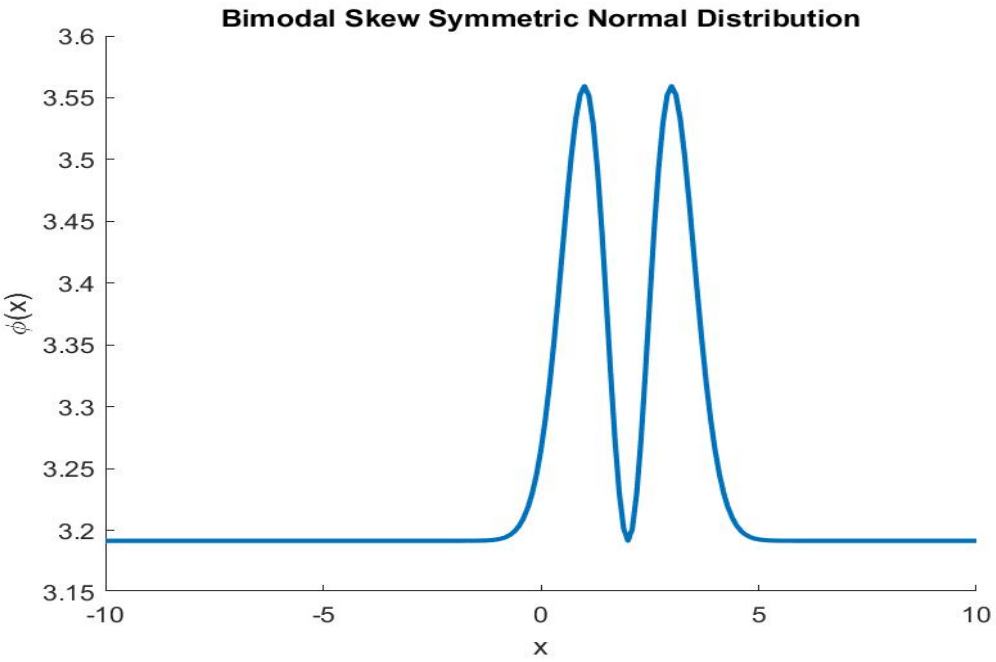

Figure 17: A general plot of Bimodal Skew-Symmetric Normal Distribution

3. CHAPTER 3
RESULT AND DISCUSSION

As we know that the bubble nuclei exhibit a special characteristic trait in their nucleon density profile, a dip near the centre. So we took several mathematical profiles (that we already described in details in CHAPTER 2), which are able to produce a similar dip at the centre for certain values of their parameter. This was done to compare this profile and find out which profile is able to replicate the nucleon density profile for these bubble nuclei the best. The major focus at the beginning was to mimic the bubble structure using the Cosh-Gaussian curve, but after several hits and trials, better mathematical models were found that were able to replicate the structure to a much better extent than the Cosh-Gaussian profile.

Their performance (Section 2 on-wards)was compared by taking 3 cases, one where Cosh-Gaussian exactly matched the charge density profile(22O nuclei neutron charge density evaluated using defRMF method), one where Cosh-Gaussian somewhat matches the profile(46Ar proton charge density evaluated using HF) and one where it fails to match the profile(34Si proton charge density evaluated using defRMF method). For all the sections below the blue line represent the experimental data plot and the red line is the closest fit by that given mathematical profile.

1 Cosh-Gaussian Profile

The analysis for the Cosh-Gaussian profile was done for all the nuclei exhibiting prominent bubble structure. The results are divided into 3 subsections namely Matching, Partially Matching and Non-matching.

1.1 Matching Results

This section contains all the plots for which our simulated cosh Gaussian curve for a certain value of the 3 unknowns a, A and Ω matches the experimentally observed bubble structure found using HF,defRMF and sph RMF(experimentally observed structure represented by

blue line and simulated by red). One thing we observe is that the bubble structure of 22O and 23F for most cases was found to have an exact fit with our simulated Cosh-Gaussian curve. Only in the case of neutron charge density found using HF did 22O and 23F didn't match the said result.

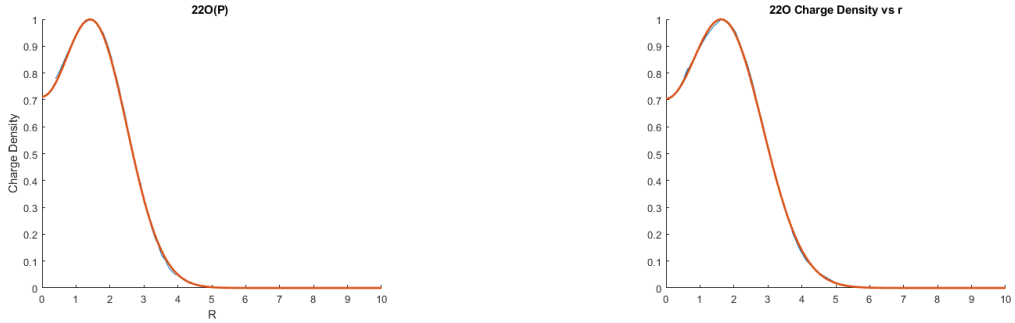

(a) Proton charge density vs Radial Distance **(b)** Neutron Charge Density vs Radial Distance

Figure 18: Charge Density plots for 22O using defRMF method.
Here the red line plot shows the closest fit plot and the blue line shows the experimental data plot. The same has been followed for the rest of the figures too.

Figure 18 depicts the variation of proton and neutron charge density of 22O with the radial distance from the centre of the nucleus. We see that the charge density plot for both nucleons matches exactly our Cosh-Gaussian profile. The method used to calculate the experimental data is Definite Relativistic Mean Field Theory (defRMF).

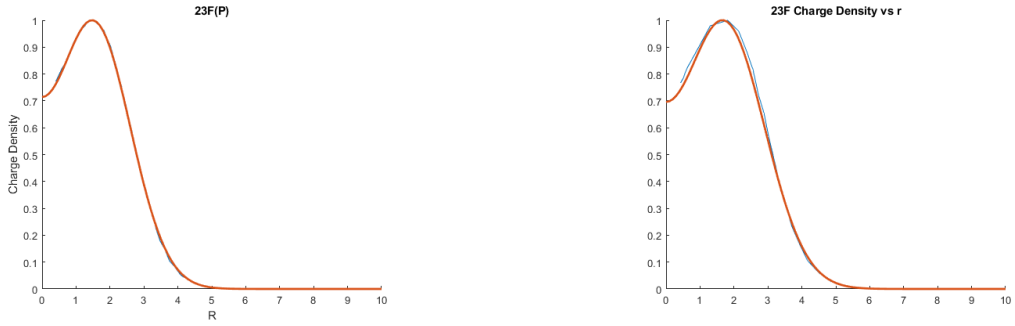

(a) Proton charge density vs Radial Distance **(b)** Neutron Charge Density vs Radial Distance

Figure 19: Charge Density plots for 23F using defRMF method.

Figure 19 compares the bubble structure obtained in nucleon charge density in 23F using

the defRMF method with our Cosh-Gaussian profile. We observe an exact fit.

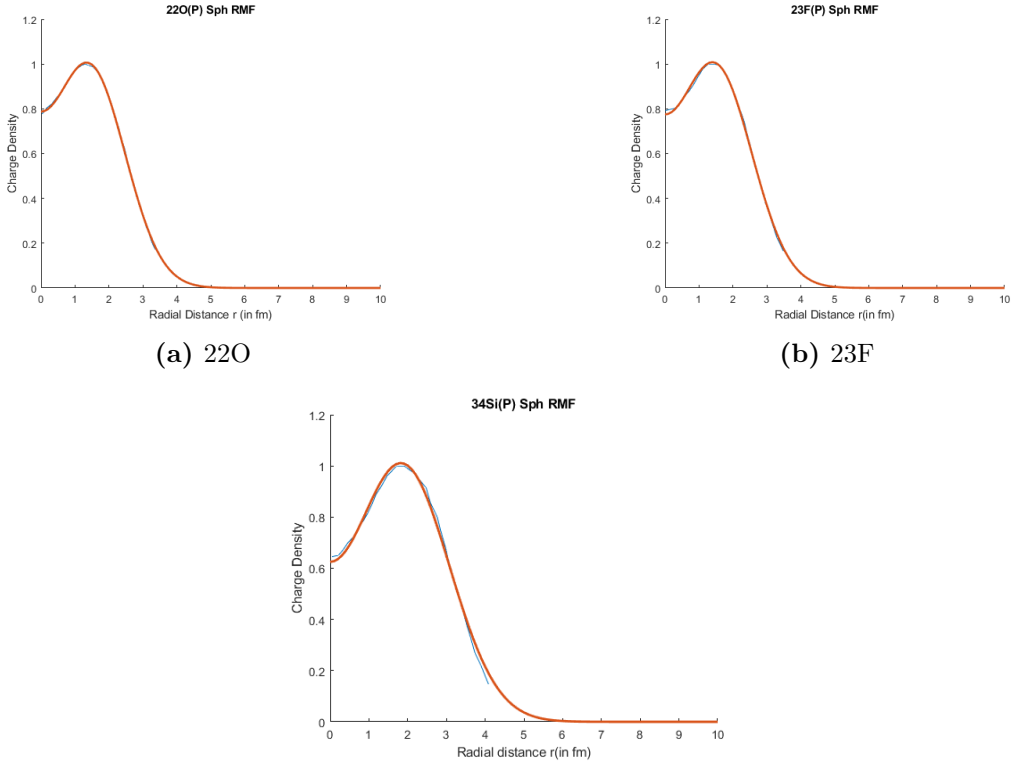

(a) 22O **(b)** 23F

(c) 34Si

Figure 20: Proton Charge Density vs Radial Distance Using Sph RMF.

By observing Figure 20 we can see that the bubble structure obtained in proton charge density when found using Spherical Relativistic Mean Field theory(Sph RMF) for the elements 22O, 23F and 34Si exactly matches our Cosh-Gaussian Profile.

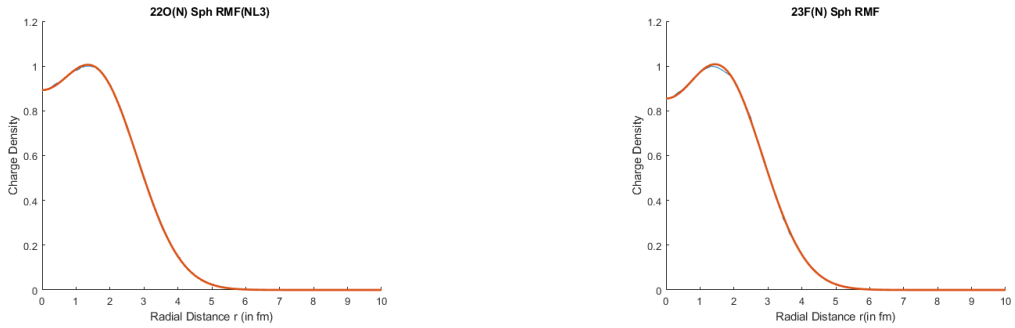

(a) 220 **(b)** 23F

Figure 21: Neutron Charge Density vs Radial Distance plots using Sph RMF method.

When Sph RMF is used to calculate the bubble structure in neutron charge density for the given elements, an exact match with the Cosh-Gaussian profile is only obtained for 220 AND 23F as shown in Figure 21

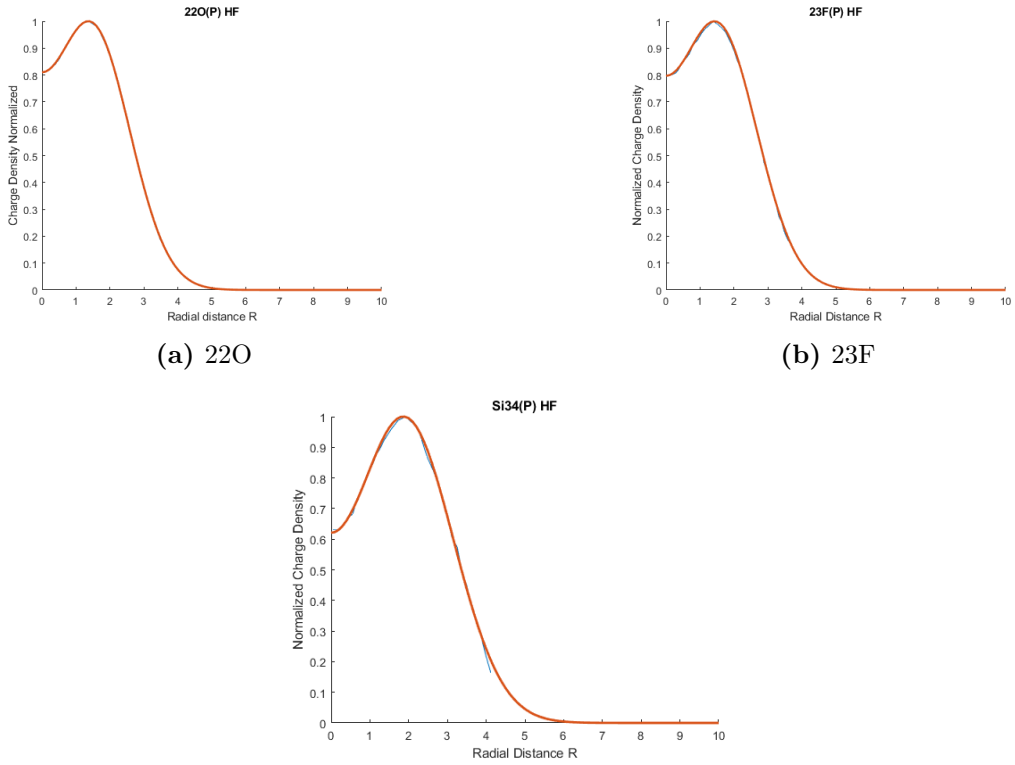

(a) 22O **(b)** 23F

(c) 34Si

Figure 22: Proton Charge Density vs Radial Distance Using Hartree Fock Method.

Finally, the Cosh-Gaussian profile is compared to the bubble structure obtained in proton

and neutron charge density for the given nuclei using the Hartree-Fock method. From Figure 22, it is observed that the bubble structure for proton charge density produces an exact match with the Cosh-Gaussian profile only for 22O, 23F and 34Si. No exact fit is obtained while comparing the Cosh-Gaussian profile with the bubble structure in neutron charge density.

1.2 Partially matching

This section contains the plots of neutron and proton charge density bubble structures with the Cosh-Gaussian curve. In these curve, the Cosh-Gaussian profile does not exactly fit the bubble structure in neutron and proton charge density but still have a very high correlation with it. The slight discrepancy is due to the value of charge density at a very small radial distance not matching the Cosh-gaussian profile.

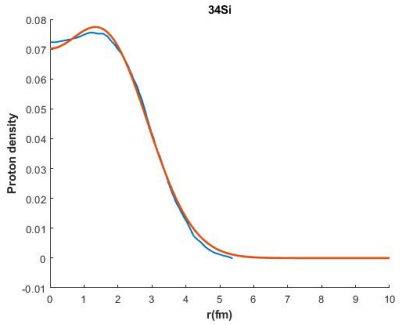

(a) 34Si

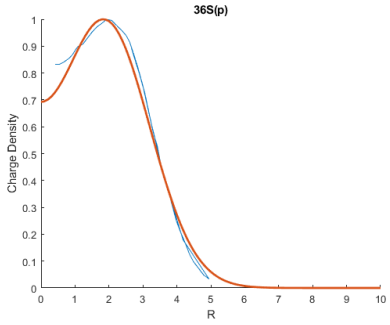

(b) 36S

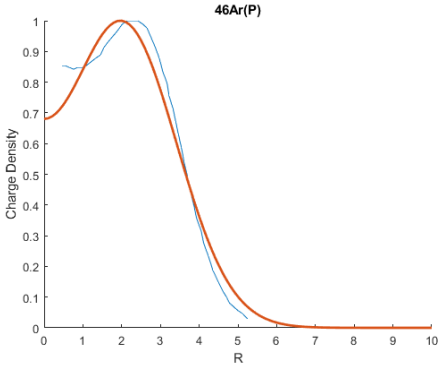

(c) 46Ar

Figure 23: Proton Charge Density vs Radial Distance Using def RMF method.

Figure 23 compares the proton charge density calculated using defRMF method with the Cosh-Gaussian profile. We can see that for the 3 curves, the discrepancy is for a small radial distance. The dip obtained at r = 0 is overestimated by the Cosh-Gaussian profile. In Figure

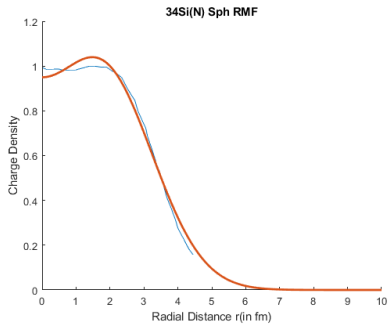

(a) Neutron Bubble structure for 34Si

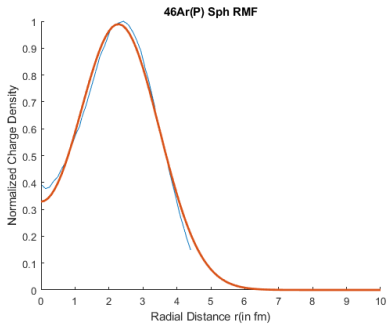

(b) Proton bubble structure for 46Ar

Figure 24: Charge Density vs Radial Distance plots using Sph RMF method.

24 we compare the proton charge density calculated using SphRMF method of the nuclei 34Si and 46Ar. In the case of 34 Si for a small radial distance, the proton charge density is nearly flat which the Cosh-Gaussian profile failed to produce while in the case of 46Ar, the Cosh-Gaussian profile overestimates the dip produced for very small r values.

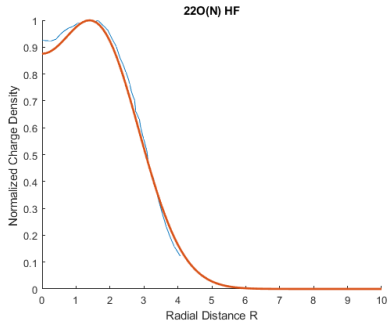

(a) Neutron Bubble Structure of 22O

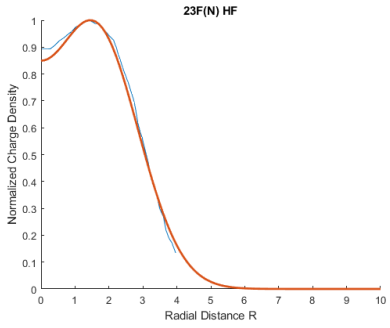

(b) Neutron Bubble Structure of 23F

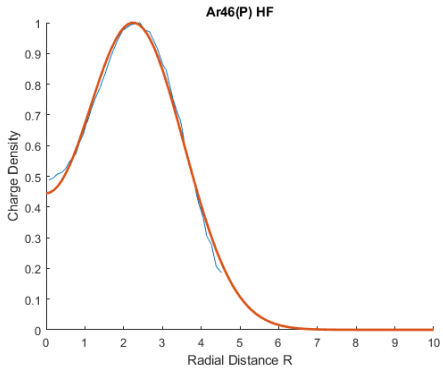

(c) Proton Bubble Structure of Ar46

Figure 25: Nucleon Charge Density vs Radial Distance Using Hartree Fock method.

In Figure 25 the bubble structure produced in proton and neutron charge density for

various nuclei is studied and compared with a Cosh-Gaussian profile. Hartree Fock's method is used to calculate the charge density of the nucleons of various nuclei. For 22O and 23F the neutron charge density differs slightly from the Cosh-Gaussian curve for small radial distance (r) values. For 46Ar the proton charge density and the Cosh-Gaussian profile show slight discrepancy for small r values. In all these cases the Cosh-Gaussian profile overestimates the dip produced at small r values.

1.3 Non Matching

These plots show a very small correlation between the Cosh-Gaussian profile and the bubble structure in proton and neutron charge density. Basically, a local minimum or a saddle point is obtained for these nuclei nucleon charge density for a certain value of r which the Cosh-Gaussian curve fails to reproduce. And hence we can classify these plots as non-matching.

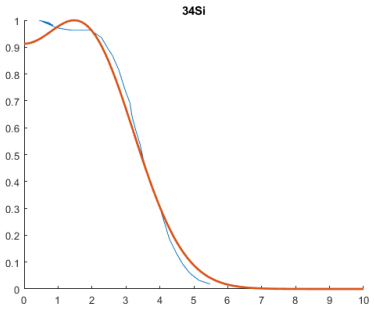

(a) 34Si Bubble Structure

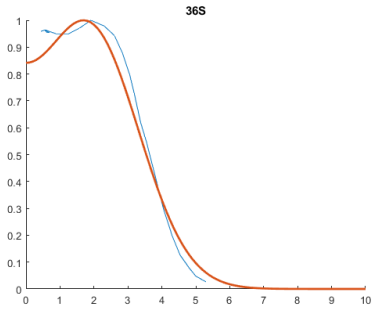

(b) 36S Bubble Structure

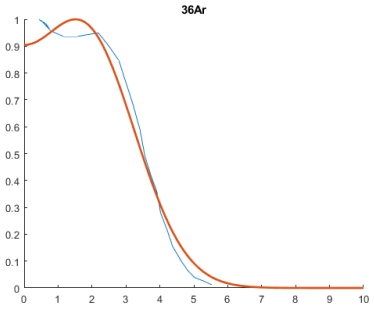

(c) 36Ar Bubble Structure

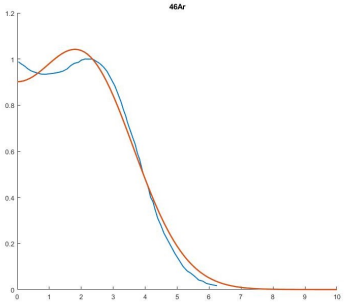

(d) 46Ar Bubble Structure

Figure 26: Neutron Charge Density vs Radial Distance Using def RMF method.

In Figure 26 we compare the neutron charge density calculated using defRMF method

with the Cosh-Gaussian profile. We observe a saddle point formation at r =2 femtometer for 34Si and 36Ar and near 2.5 fm for 36S and 46 Ar. The Cosh-Gaussian profile can reproduce this saddle point and hence fails to match the experimental plots.

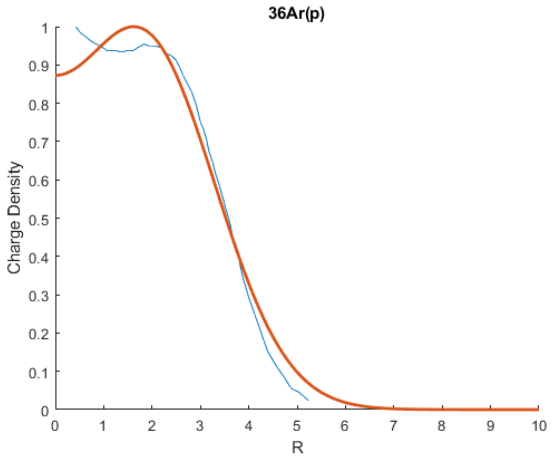

(a) 36Ar Bubble Structure

Figure 27: Proton Charge Density vs Radial Distance Using def RMF method.

In figure 27 we compare the proton charge density plot for 36Ar calculated using def RMF method with the Cosh-Gaussian profile Here once again a saddle point is observed experimentally at r = 2 fm which the profile fails to match.

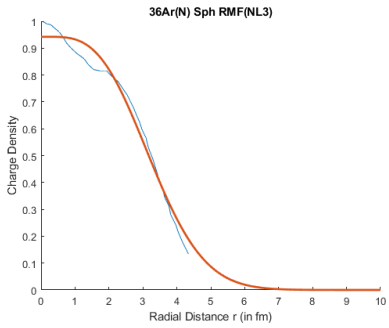

(a) Bubble Structure of 36Ar

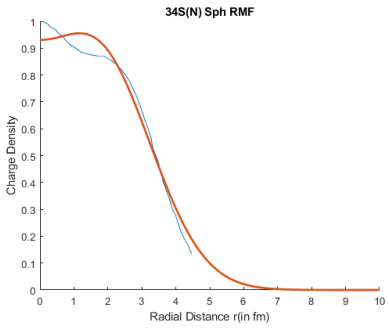

(b) Bubble Structure of 36S

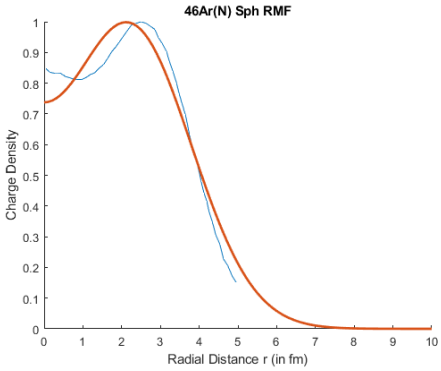

(c) Neutron Bubble Structure of 46Ar

Figure 28: Neutron Charge Density vs Radial Distance Using Sph RMF method.

Figure 28 compares the neutron charge density calculated using SphRMF method with the Cosh-Gaussian profile for 36Ar,36S and 46Ar. A local minima is observed at points near $r = 1.8$ fm in cases of 36S , between 1 to 2.5 fm for 3Ar and at r 1.5 fm for 46Ar.

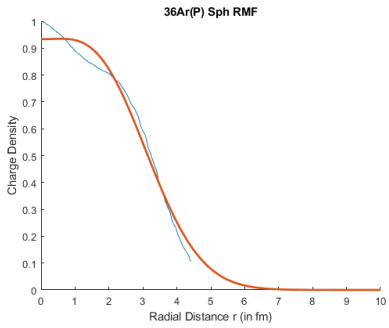

(a) Bubble Structure 36 Ar

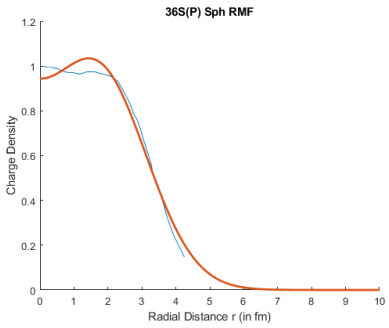

(b) Bubble Structure 36S

Figure 29: Proton Charge Density vs Radial Distance using Sph RMF method.

Proton charge density is calculated using the SphRMF method and compared with the Cosh-Gaussian profile. Referring to Figure 29, it is observed that a saddle point formation

takes place in the case of 36 Ar at around 1.5 to 1.9 fm. While in the case of 36S, a flat top is observed for a smaller radial distance r.

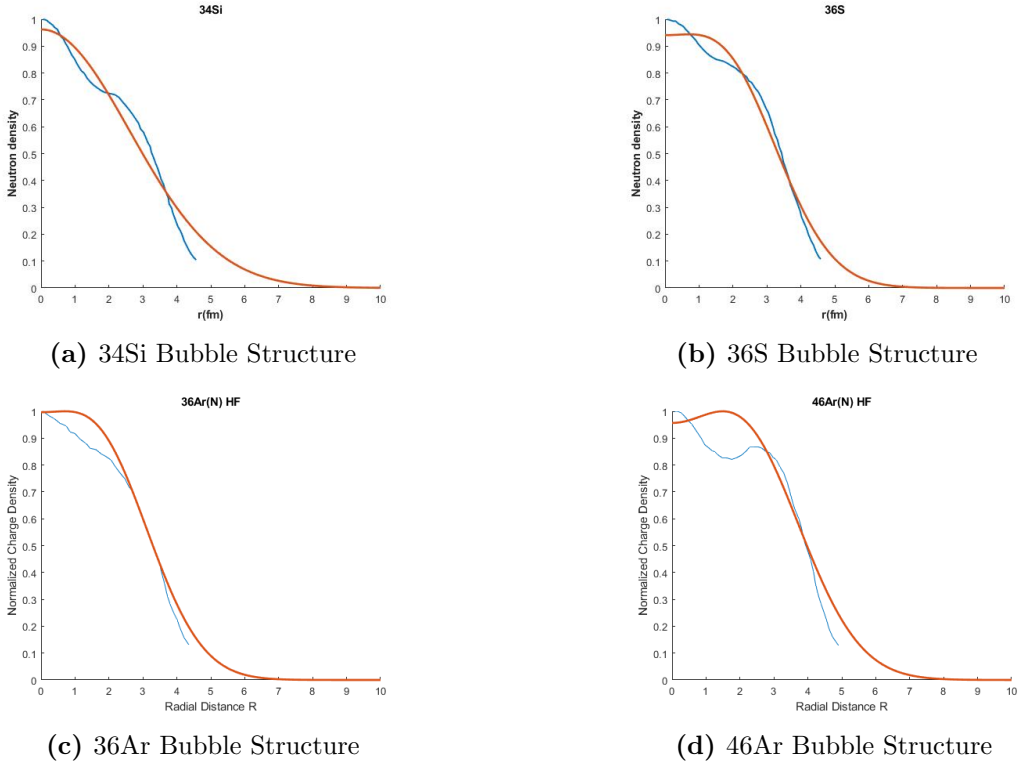

(a) 34Si Bubble Structure

(b) 36S Bubble Structure

(c) 36Ar Bubble Structure

(d) 46Ar Bubble Structure

Figure 30: Neutron Charge Density vs Radial Distance Using Hartree Fock method.

At last proton and neutron charge density calculated using the Hartree Fock method is compared with the Cosh-Gaussian profile. Figure 30 bubble structure in the neutron charge density is compared with the Cosh-Gaussian profile. In all the given cases, a dip in the expected charge density value occurs at smaller radial distances which the profile fails to match.

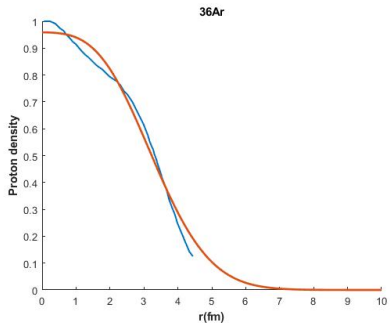

(a) Bubble Structure 36 Ar

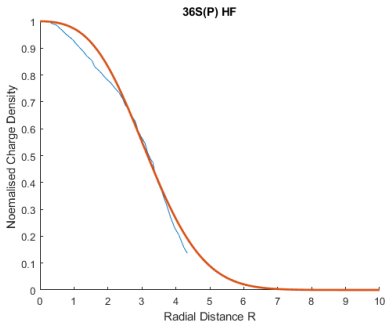

(b) Bubble Structure 36S

Figure 31: Proton Charge Density vs Radial Distance using Hartree Fock Method.

Figure 31 compares the bubble structure obtained in the proton charge density of 36Ar and 36S with the Cosh-Gaussian profile. Ignoring the straight line observed in 36 Ar saddle point formation occurs at a smaller radial distance. While for 36 S a good co-relation is found except at a smaller radial distance where the experimental proton charge density has a slight dip.

2 Ricker Wavelet or Mexican hat wavelet

Mexican hat wavelet profile or the Ricker wavelet was used to plot the charge density and neutron density profile for the 3 nuclei 220(neutron density using defRMF), 34Si(Neutron density using defRMF) and 46Ar(proton density using HF).

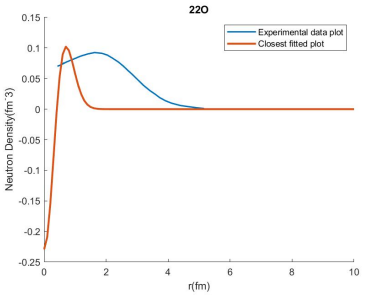

Figure 32: Neutron Charge density vs Radial distance for 22O

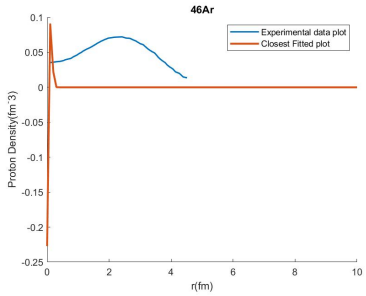

Figure 33: Proton Charge density vs radial distance for 46 Ar

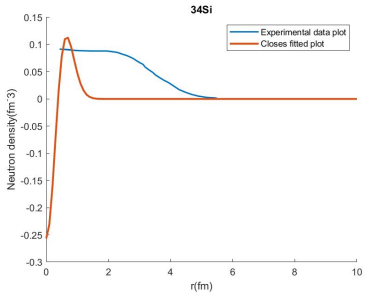

Figure 34: Neutron Charge density vs radial distance for 34Si

The results obtained are not very promising. Even though it was able to produce a dip for very small radial distances, it failed to match the width of the bubble structure for all

the cases.

3 Cauchy Distribution

Cauchy distribution was used to plot the charge density and neutron density vs radial distance for the same nuclei i.e. 22O(Neutron density defRMF),34Si(Neutron density defRMF) and 46Ar(Proton density HF).

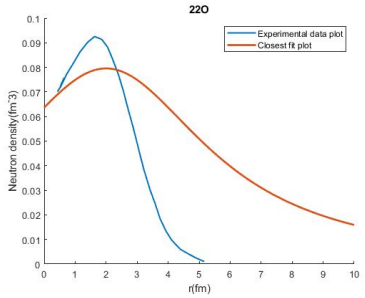

Figure 35: Neutron Charge density vs Radial distance for 22O

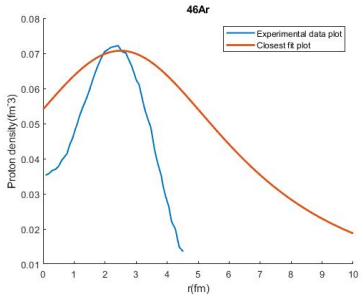

Figure 36: Proton Charge density vs radial distance for 46 Ar

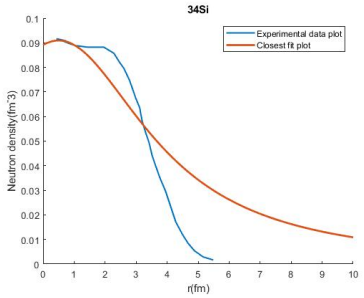

Figure 37: Neutron Charge density vs radial distance for 34Si

From the above figure, we can say the Cauchy distribution did a somewhat better job than the ricker wavelet function but still was not able to exactly replicate any of the given bubble structures. A central dip was produced by the rise and fall of the Gaussian-like curve could not be replicated

4 Laplace Distribution

Laplace distribution was also used to compute the nucleon density vs radial distance plots for the before-mentioned nuclei and their performance compared.

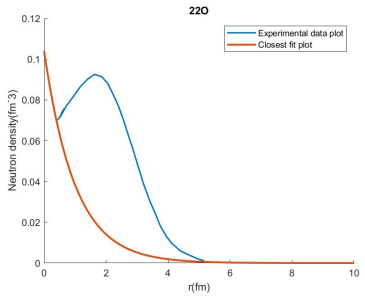

Figure 38: Neutron Charge density vs Radial distance for 22O

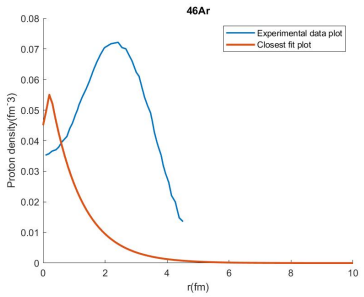

Figure 39: Proton Charge density vs radial distance for 46 Ar

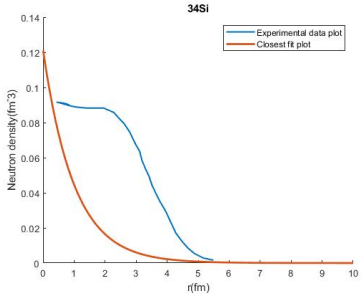

Figure 40: Neutron Charge density vs radial distance for 34Si

We see a very poor performance by the Laplace distribution while replicating the bubble structure. In most cases, it could not even replicate the dip observed in the charge density distribution. A dip was observed in the case of Ar46 but the matching with the proton density was subpar.

5 Raised Cosine filter/function

Raised cosine filter is mostly used in digital communications as a nyquist low pass filter but here we tested it as a suitable candidate for representing the bubble structure.

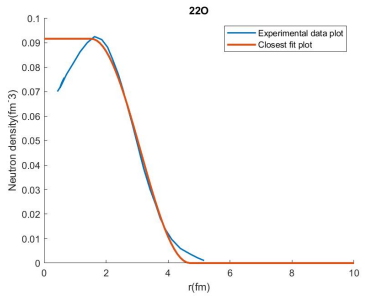

Figure 41: Neutron Charge density vs Radial distance for 22O

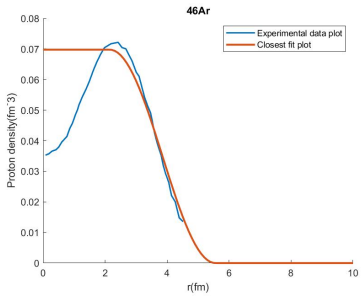

Figure 42: Proton Charge density vs radial distance for 46 Ar

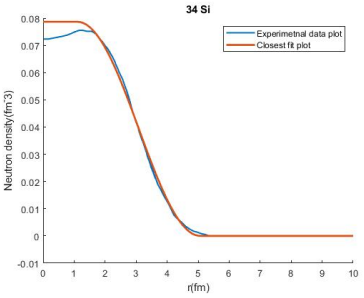

Figure 43: Neutron Charge density vs radial distance for 34Si

From the above figure, we can see even though the raised cosine function cant produce a dip, it does match the falling edge of the bubble structure plot in all cases. In the case of 34Si, the neutron density vs radial density plot obtained by Raised cosine profile is in fact better than the Cosh-Gaussian profile.

6 Normal distribution

The normal distribution has once again found its utility, now in predicting the nucleon density plot for the bubble nuclei.

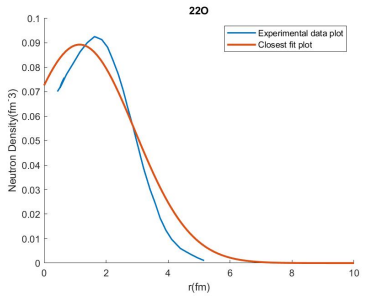

Figure 44: Neutron Charge density vs Radial distance for 22O

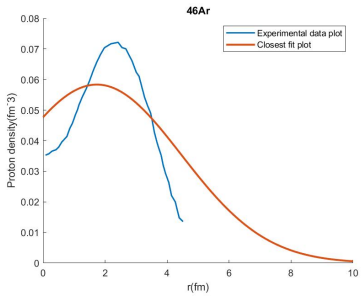

Figure 45: Proton Charge density vs radial distance for 46 Ar

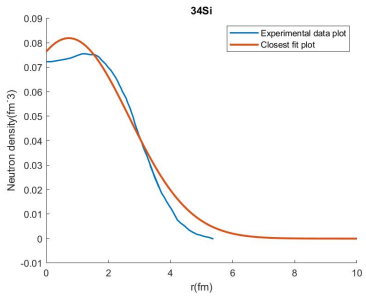

Figure 46: Neutron Charge density vs radial distance for 34Si

Even though normal distribution is unimodal its mean value can be varied to produce a central dip. It did a somewhat good job of matching the experimental nucleon density profile for the given bubble nuclei but fails when there is a sharp change in slope or a flat slope in the density profile.

7 Gompertz Function

Gompertz function was used to replicate or match the nucleon density profile for before-mentioned bubble nuclei.

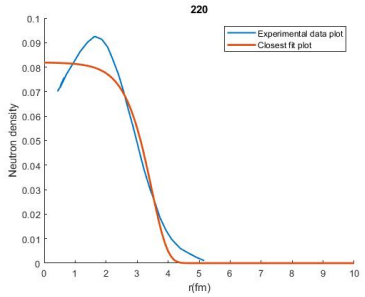

Figure 47: Neutron Charge density vs Radial distance for 22O

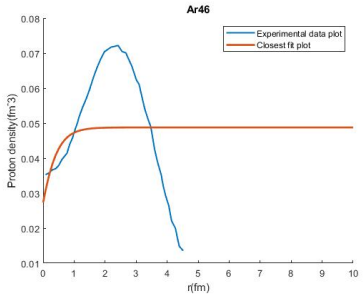

Figure 48: Proton Charge density vs radial distance for 46 Ar

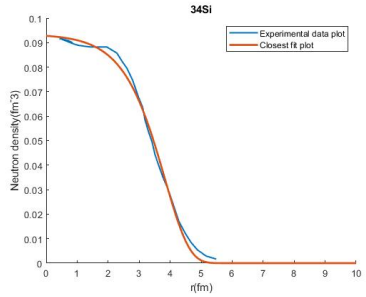

Figure 49: Neutron Charge density vs radial distance for 34Si

Gompertz function showed satisfactory results in some cases(34Si) and poor results in some cases(Ar46). It was not able to produce a central dip in most cases but did match the falling edge of most bubble structures. In cases where the curvature was sharp, it failed to even match the falling edge.

8 Modified Bessel Function of the second kind

We did not actually use the modified function of the second kind rather we took its derivative(with respect to the independent variable).

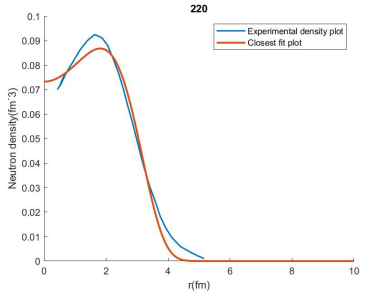

Figure 50: Neutron Charge density vs Radial distance for 22O

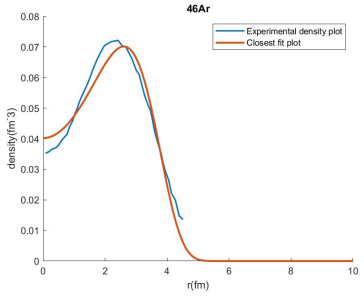

Figure 51: Proton Charge density vs radial distance for 46 Ar

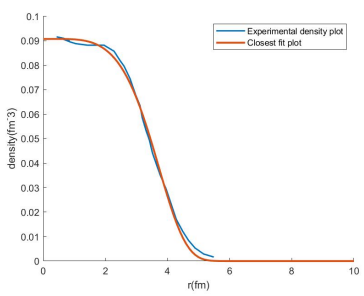

Figure 52: Neutron Charge density vs radial distance for 34Si

The result as seen in the above figure is adequate to assume that the derivative of the Bessel function of 2nd kind does a good job in replication of the nucleon density profile of various bubble nuclei. The result is comparable to the Cosh-Gaussian profile. While the matching in the case of 22O is worse than that of the Cosh-Gaussian function, it does a better job of replicating the neutron density profile for 34Si.

9 Conway-Maxwell Poisson Distribution

Conway-Maxwell Poisson distribution was analyzed by comparing its performance with various mathematical profiles in producing the closest fit for the nucleon density profile for various bubble nuclei.

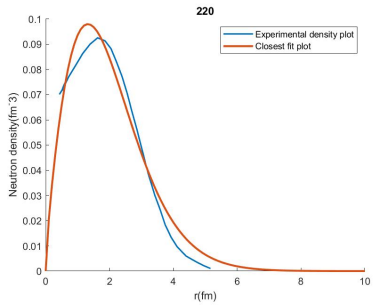

Figure 53: Neutron Charge density vs Radial distance for 22O

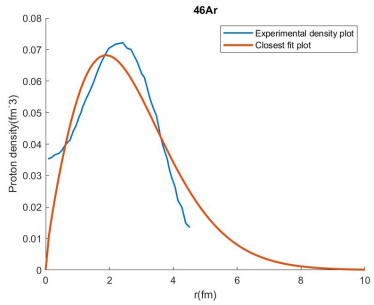

Figure 54: Proton Charge density vs radial distance for 46 Ar

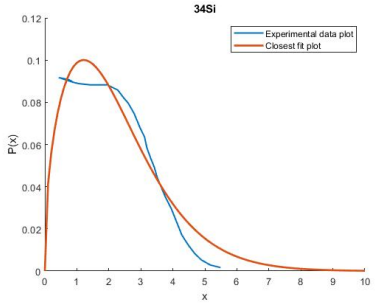

Figure 55: Neutron Charge density vs radial distance for 34Si

Conway-Maxwell Poisson distribution(CMPD) is able to produce a central dip in all cases but the dip goes to zero for all the cases. In cases where the dip is not prominent(34Si) it fails to replicate the same. Overall the performance of CMPD is average when compared to others.

10 Bimodal Skew-Symmetric Normal Distribution

The best performing mathematical profile of them all. Bimodal Skew-Symmetric Normal distribution was able to match all the profiles that were given to it. Therefore to check its performance all 36 profiles were taken (similar to the Cosh-Gaussian function).

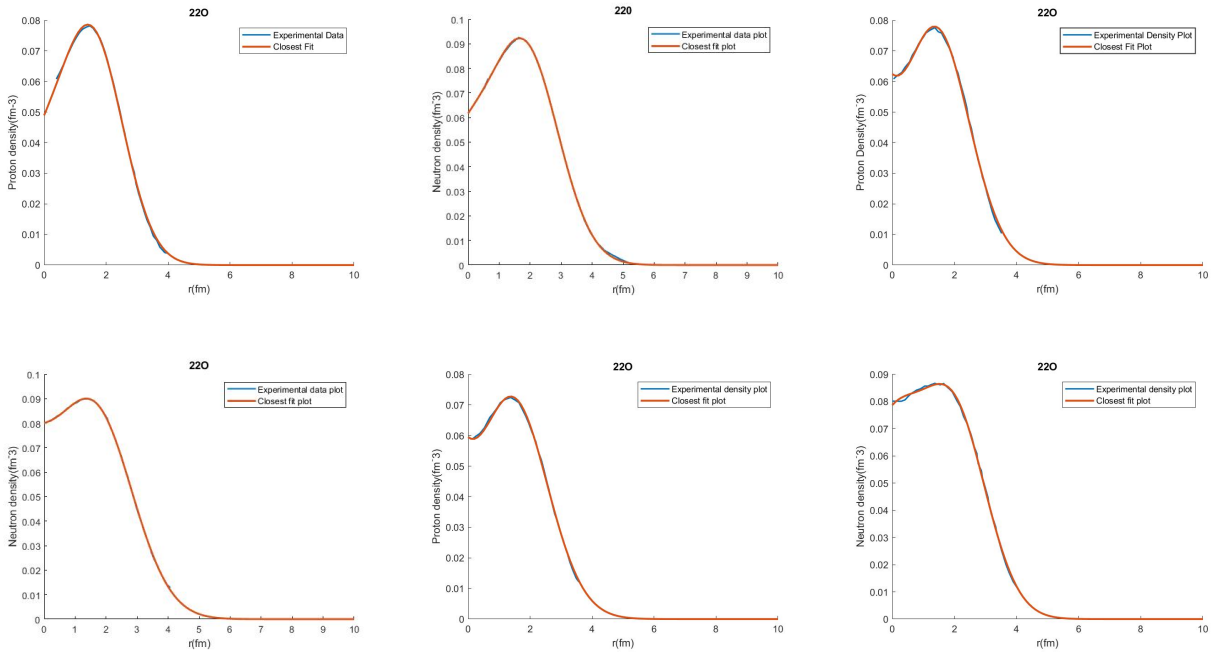

Figure 56: Proton and neutron density plot for 22O using defRMF,Sph RMF and Hartree-Fock method compared with Bimodal Skew-Symmetric Normal Distribution

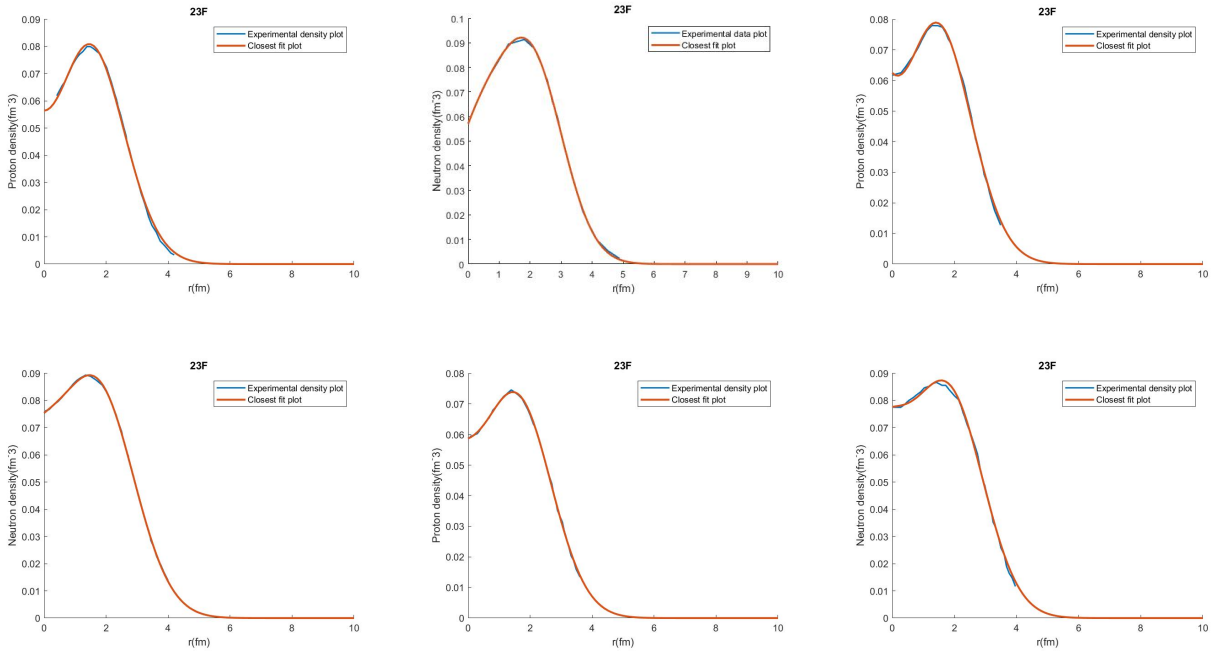

Figure 57: Proton and neutron density plot for 23F using defRMF, Sph RMF and Hartree-Fock method compared with Bimodal Skew-Symmetric Normal Distribution

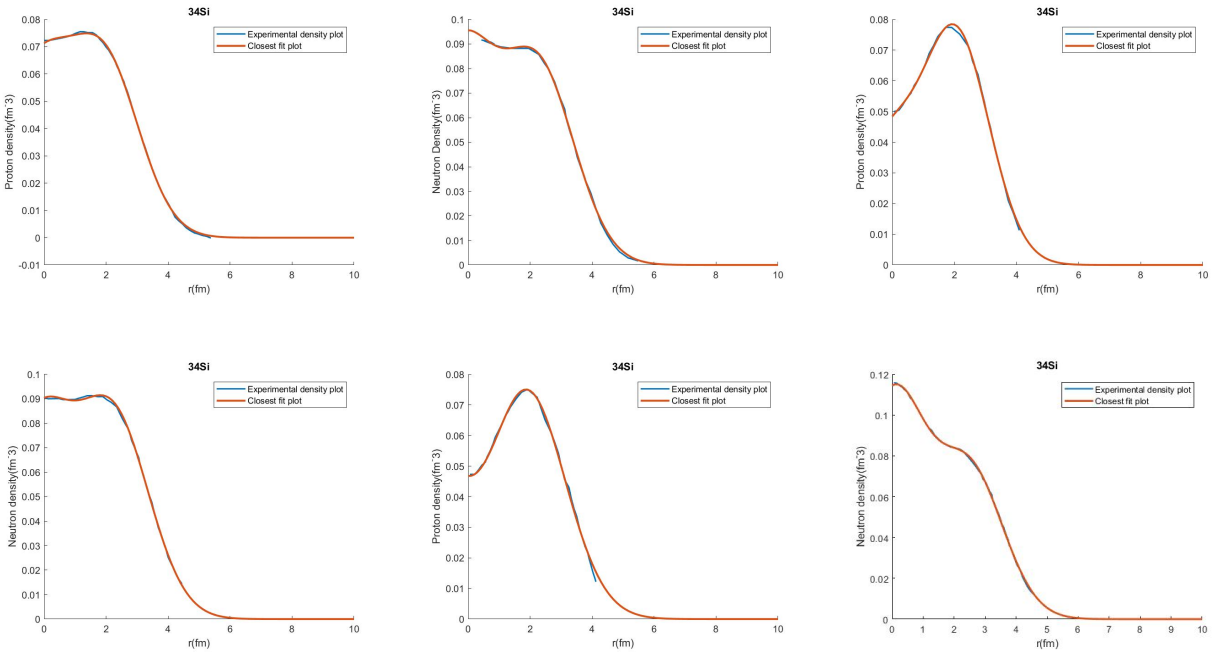

Figure 58: Proton and neutron density plot for 34Si using defRMF, Sph RMF and Hartree-Fock method compared with Bimodal Skew-Symmetric Normal Distribution

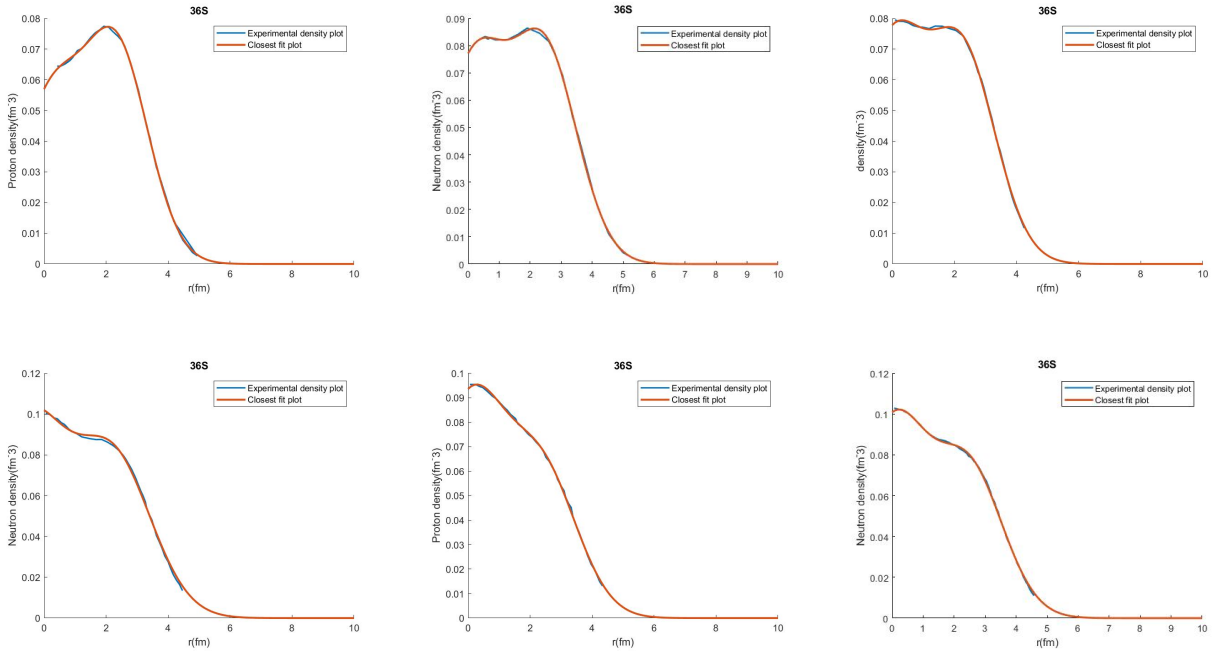

Figure 59: Proton and neutron density plot for 36S using defRMF, Sph RMF and Hartree-Fock method compared with Bimodal Skew-Symmetric Normal Distribution

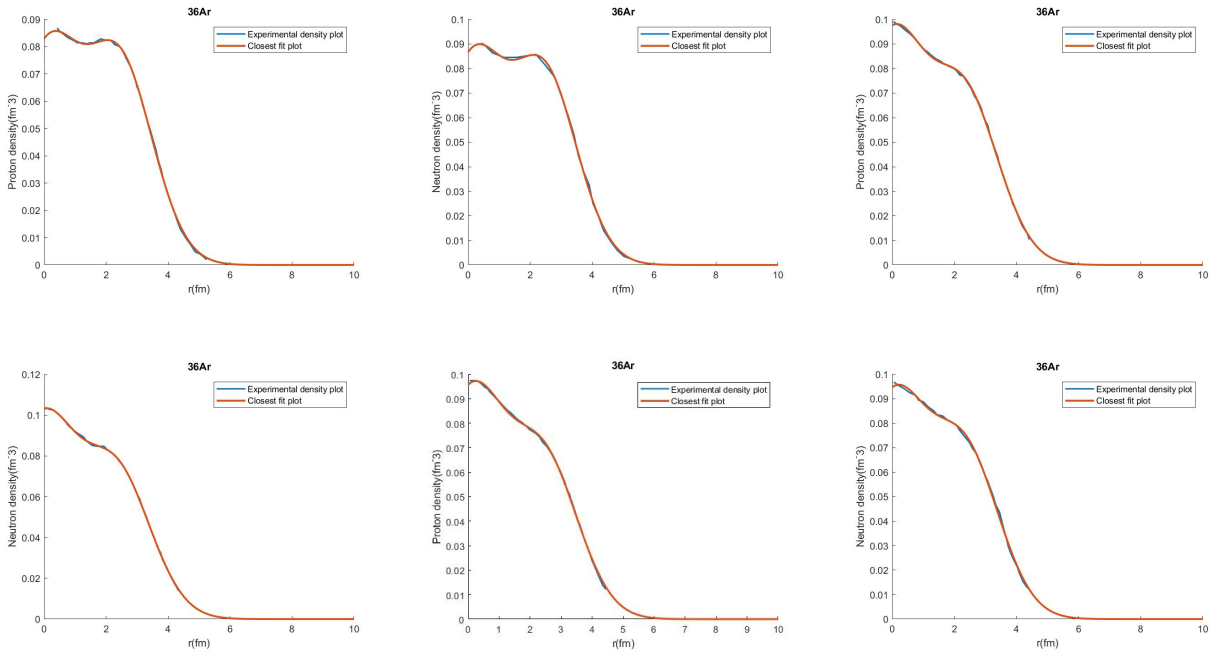

Figure 60: Proton and neutron density plot for 36Ar using defRMF, Sph RMF and Hartree-Fock method compared with Bimodal Skew-Symmetric Normal Distribution

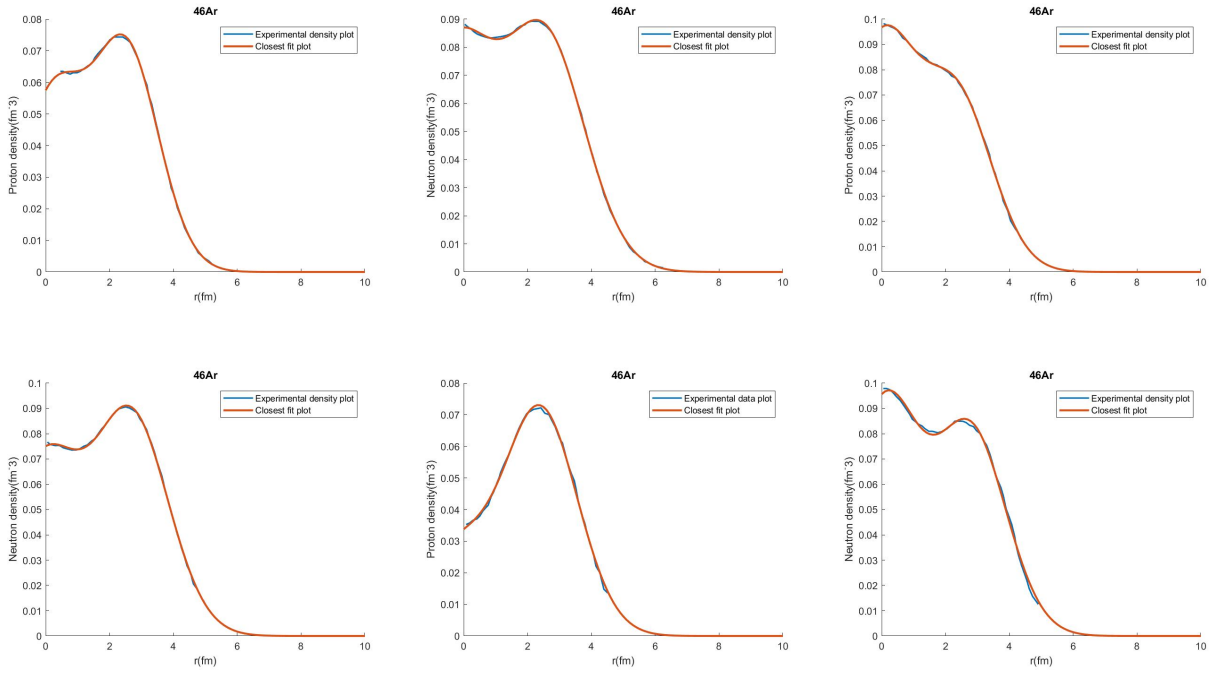

Figure 61: Proton and neutron density plot for 46Ar using defRMF, Sph RMF and Hartree-Fock method compared with Bimodal Skew-Symmetric Normal Distribution

From all the above plots we see that there is hardly any case where Bimodal Skew-Symmetric Normal distribution failed to replicate exactly the nucleon density profile. From this, we can conclude that the Bimodal Skew-Symmetric Normal Distribution is the best mathematical profile amongst the rest we have used to evaluate various nucleon density profiles.

4. CONCLUSION AND FUTURE SCOPE

A bubble nucleus has a paucity of neutron and proton density at the centre of the nucleus. Therefore, when both the mass and charge density profiles are plotted against radial distance, a central dip is observed. Tedious numerical methods have been employed to reveal the bubble nucleus profile, which is complicated and cumbersome. Now the selection of the mathematical profiles is based on them having a central dip . In this thesis, we investigated the possibility of correlating the mathematical profiles with the density profile of bubble nuclei. Ten different families of mathematical profiles were considered. Out of all these mathematical profiles

Bimodal skew-symmetric normal distribution emerged as the best matching profile, while Cosh-Gaussian performed well in some cases where the bubble structure was more prominent. Other than these 2, the derivative of the modified Bessel function of the second kind also performed well for the cases given. While the Laplace distribution, the Cauchy distribution and the Ricker wavelet performed very poorly. The performance of mathematical profiles like the Raised cosine function, the normal distribution, the Gompertz curve and the Conway-Maxwell Poisson distribution were totally case-dependent, performing very well in some cases and poorly in others.

The investigation results raise a new question: whether a general mathematical form of a profile can be developed for all the bubble density profiles. To answer this, one can further investigate the nucleus density profile through a machine learning approach however the immediate challenge is a lesser number of samples i.e. nucleus profiles which can be overcome by adopting different potential profiles for a single nucleus, therefore all nuclei, whether bubble or not and a good number of potential profiles after various permutation and combinations may create the required volume of initial data for machine learning approach.

References

[1] Kenneth S Krane. *Introductory nuclear physics*. John Wiley & Sons, 1991.

[2] Simon Saunders. Fermi-dirac statistics. In *Compendium of Quantum Physics*, pages 230–235. Springer, 2009.

[3] Sven Gosta Nilsson and Ingemar Ragnarsson. *Shapes and Shells in Nuclear Physics*. Cambridge University Press, 1995.

[4] J.A. Wheeler. Nucleonics notebook. unpublished, 1950.

[5] J.A. Wheeler R. Euwema. unpublished.

[6] BG Todd-Rutel, Jorge Piekarewicz, and PD Cottle. Spin-orbit splitting in low-j neutron orbits and proton densities in the nuclear interior. *Physical Review C*, 69(2):021301, 2004.

[7] G. Burgunder. *Étude de l'interaction nucléaire spin-orbite par réactions de transfert* $^{36}S(d,p)^{37}S$ *et* $^{34}Si(d,p)^{35}Si$. Theses, Université de Caen, December 2011.

[8] E Khan, M Grasso, J Margueron, and Nguyen Van Giai. Detecting bubbles in exotic nuclei. *Nuclear Physics A*, 800(1-4):37–46, 2008.

[9] Akhilesh Yadav, A Shukla, V Kumar, DN Kadrev, and MK Gaidarov. Semi-bubble structure of superheavy nuclei. *Modern Physics Letters A*, 37(20):2250130, 2022.

[10] S.K. Patra S.K. Singh, M. Ikram. *Int. J. Mod. Phys. E, 22 (2012), Article 135001*, 2012.

[11] M. Ikram, S.K. Singh, A.A. Usmani, and S.K. Patra. A relativistic mean field study of multi-strange system. *International Journal of Modern Physics E*, 23(9), 2014. Cited by: 10; All Open Access, Green Open Access.

[12] Michael Bender and Paul-Henri Heenen. Structure of superheavy nuclei. In *Journal of Physics: Conference Series*, volume 420, page 012002. IOP Publishing, 2013.

[13] Adam Sobiczewski and Krzysztof Pomorski. Description of structure and properties of superheavy nuclei. *Progress in Particle and Nuclear Physics*, 58(1):292–349, 2007.

[14] J Dechargé, J-F Berger, K Dietrich, and MS Weiss. Superheavy and hyperheavy nuclei in the form of bubbles or semi-bubbles. *Physics Letters B*, 451(3-4):275–282, 1999.

[15] L. Tan Phuc, N. Quang Hung, and N. Dinh Dang. Bubble nuclei within the self-consistent hartree-fock mean field plus pairing approach. *Physical Review C*, 97(2), 2018. Cited by: 7.

[16] G Saxena, M Kumawat, M Kaushik, SK Jain, and Mamta Aggarwal. Bubble structure in magic nuclei. *Physics Letters B*, 788:1–6, 2019.

[17] L Tan Phuc, N Quang Hung, and N Dinh Dang. Bubble nuclei within the self-consistent hartree-fock mean field plus pairing approach. *Physical Review C*, 97(2):024331, 2018.

[18] G Saxena, M Kumawat, BK Agrawal, and Mamta Aggarwal. Anti-bubble effect of temperature & deformation: A systematic study for nuclei across all mass regions between a= 20–300. *Physics Letters B*, 789:323–328, 2019.

[19] Shailesh K Singh, M Ikram, SK Biswal, M Bhuyan, and SK Patra. Comparative study of the effective force parameters nl3 and nl3. In *Proceedings of the DAE Symp. on Nucl. Phys*, volume 58, page 116, 2013.

[20] P G Reinhard. The relativistic mean-field description of nuclei and nuclear dynamics. *Reports on Progress in Physics*, 52(4):439, apr 1989.

[21] D Gogny and Pierre-Louis Lions. Hartree-fock theory in nuclear physics. *ESAIM: Mathematical Modelling and Numerical Analysis*, 20(4):571–637, 1986.

[22] Munish Aggarwal, Shivani Vij, and Niti Kant. Propagation of cosh gaussian laser beam in plasma with density ripple in relativistic–ponderomotive regime. *Optik*, 125(18):5081–5084, 2014.

[23] S Kaur, M Kaur, R Kaur, and TS Gill. Propagation characteristics of hermite-cosh-gaussian laser beam in a rippled density plasmas. *Laser and Particle Beams*, 35(1):100–107, 2017.

[24] Guoquan Zhou and Fengqin Liu. Far field structural characteristics of cosh-gaussian beam. *Optics & Laser Technology*, 40(2):302–308, 2008.

[25] Navpreet Singh, Naveen Gupta, and Arvinder Singh. Second harmonic generation of cosh-gaussian laser beam in collisional plasma with nonlinear absorption. *Optics Communications*, 381:180–188, 2016.

[26] H Rezapour, H Zahed, and P Mokhtary. Self-focusing and defocusing of cosh gaussian laser beam in the presence of nonlinearity of ponderomotive force and temperature gradient. *Chinese journal of physics*, 56(5):1834–1844, 2018.

[27] Halil T Eyyuboğlu. Annular, cosh and cos gaussian beams in strong turbulence. *Applied Physics B*, 103:763–769, 2011.

[28] Halil Tanyer Eyyuboğlu and Yahya Baykal. Analysis of reciprocity of cos-gaussian and cosh-gaussian laser beams in a turbulent atmosphere. *Optics Express*, 12(20):4659–4674, 2004.

[29] Xiuxiang Chu. Propagation of a cosh-gaussian beam through an optical system in turbulent atmosphere. *Optics Express*, 15(26):17613–17618, 2007.

[30] Guoquan Zhou. Propagation of a higher-order cosh-gaussian beam in turbulent atmosphere. *Optics express*, 19(5):3945–3951, 2011.

[31] Halil T Eyyuboğlu and Yahya Baykal. Transmittance of partially coherent cosh-gaussian, cos-gaussian and annular beams in turbulence. *Optics communications*, 278(1):17–22, 2007.

[32] Takashi Takekawa. Fast parallel calculation of modified bessel function of the second kind and its derivatives. *SoftwareX*, 17:100923, 2022.

[33] MY Hassan and MY El-Bassiouni. Bimodal skew-symmetric normal distribution. *Communications in Statistics-Theory and Methods*, 45(5):1527–1541, 2016.

5. Appendix

The Cosine Hyberbolic Gaussian (Cosh-Gaussian) profile finds many applications in the present world. One of those applications has been the main focus of the present thesis. We tried to estimate the bubble structure found in the nucleus of mainly 22O,23F,34Si,36Ar,36S, and 46Ar using the Cosh-Gaussian profile by varying its parameter. These sets of elements are used as they show a prominent bubble structure. Our equation for Cosh-Gaussian is

$$Y = A_0 \ \cosh(\Omega \ r/a) \exp(-r^2/2a^2)$$

Here the parameters that are varied are Ω, A_0 and a . These parameters can produce a definite peak and dip observed in the bubble nuclei of the before-mentioned elements. Peak is defined as the maximum value the curve can obtain and dip is defined as the difference between the peak value and the central minima obtained for a given Cosh-Gaussian profile.

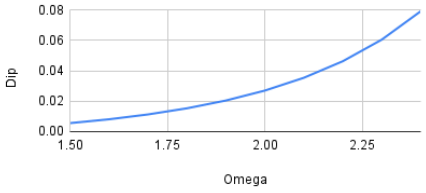

(a) Dip vs Ω Curve

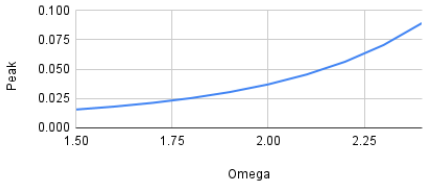

(b) Peak vs Ω Curve

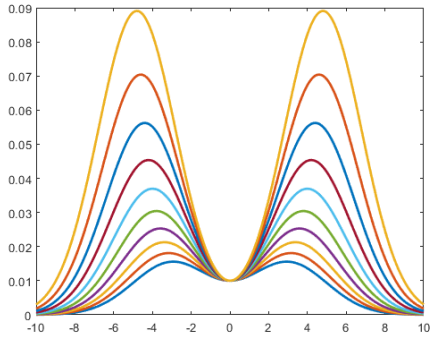

(c) Ω Variation with radial distance

Figure 62: For fixed parameter A=0.01 and a=2

Figure 62 depicts the variation in dip and peak obtained as the omega value increases, keeping the value of A and a fixed to 0.01 and 2, respectively.

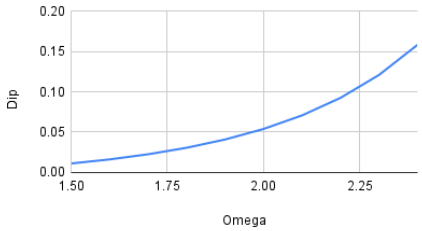

(a) Dip vs Ω curve

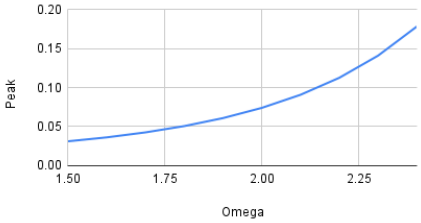

(b) Peak vs Ω Curve

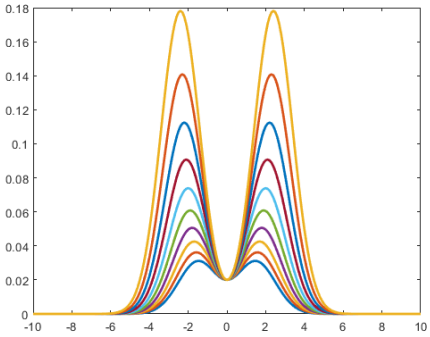

(c) Various Ω Plots with radial distance

Figure 63: Fixed Parameters A=0.02 and a=1

Figure 63 shows the relation between Ω and Dip and peak for a different value of A and a(0.02 and 1 respectively).

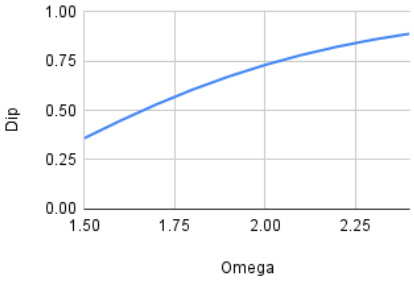

(a) Dip vs Ω plots

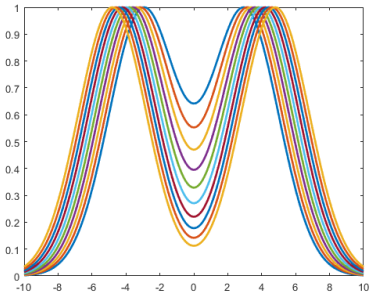

(b) Omega vs Radial Distance Plots

Figure 64: For Normalized Peak and fixed parameter A=0.01 and a =2

Here we have normalized our Cosh-Gaussian profile by diving each Ω plot by their respective peak value so that we can solely focus on the dip and Ω relation. The parameters A and a are fixed to values 0.01 and 2 respectively.

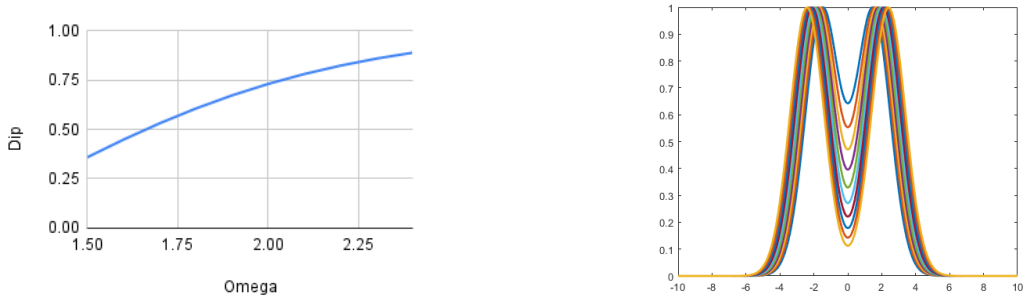

(a) Dip vs Ω Plots

(b) Ω vs Radial Distance Plots

Figure 65: For normalized peak and fixed parameter A=0.02 and a=1

Figure 65 presents the dip vs Ω relation as we set the fixed parameters to values A=0.02 and a=1.

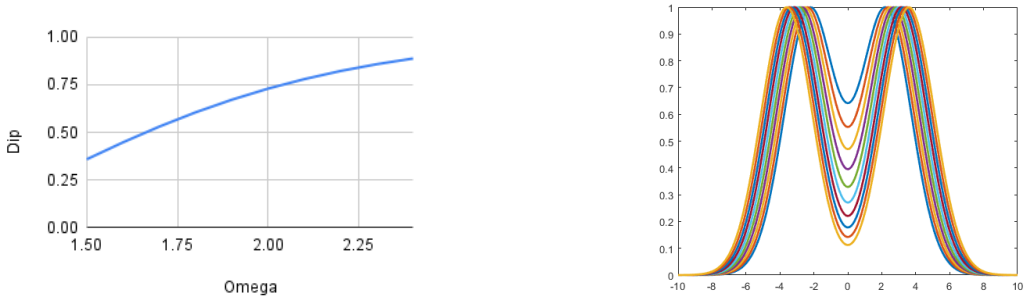

(a) Dip vs Ω plots

(b) Ω Plots with radial distance

Figure 66: For normalized peak and fixed parameter A=1 and a=1.5

Here the values of parameter A and a are and is 1.5 respectively.

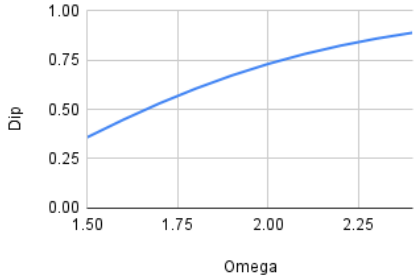

(a) Dip vs Ω Plots

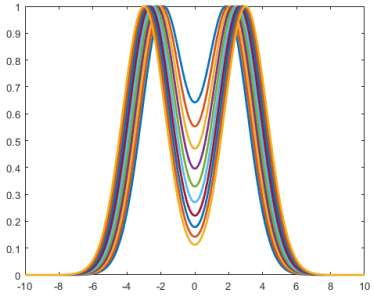

(b) Ω vs Radial distance plots

Figure 67: For normalized peak and fixed parameters A=0.075 and a =1.25

In Figure 67 the fixed parameters are set at A = 0.075 and a = 1.25.

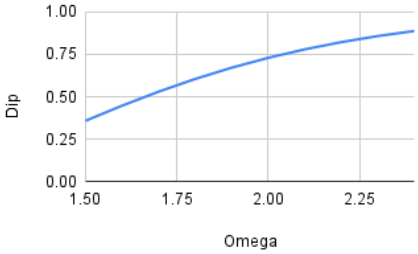

(a) Dip vs Ω plot

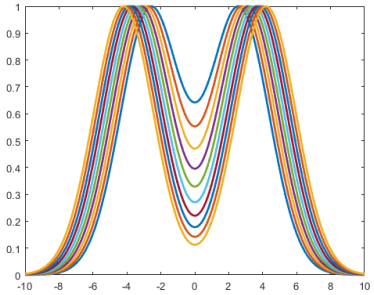

(b) Ω vs Radial distance plots

Figure 68: For normalized peak and fixed parameters A=0.075 and a=1.75

Figure 68 depicts the Ω vs Dip relation for the fixed parameters A=0.075 and a=1.75 . Drawing some conclusions from all these plots, we observe that dip and peak value increases non-linearly and is independent of the fixed parameter values.

From Figure 62 and Figure 63, we observe that the dip and peak value increases as the Ω value is increased. For a non-normalized Cosh-Gaussian profile, the value of A decides the value of the central local minima or the saddle point we observe for different Ω values. For example, in Figure 62 the central minima for various values of Ω is fixed at 0.01 which is also the value of A. Similarly, in Figure 63 the saddle point value equals our A value of 0.02. Parameter a value decides the full-width half maxima value for different Ω plots. A higher value of parameter a decreases the value exponential term in the Cosh-Gaussian profile, which in term increases the width of our plots.

In Figure 64,65,66,67,68 we have used a normalized Cosh-Gaussian curve. Normalized curves have a peak value of unity. The central local minima (saddle point)in these curves is no longer equal to the value of parameter A and is, in fact independent of the value of parameter A. The value of parameter a still defines the full width at half maxima value(FWHM) of the curves, and a larger value of a means a higher value of FWHM. From the Ω vs radial distance plots for different values of A, we see that the value of saddle point decreases as Ω value increases. That means the dip value increases as the Ω value increases. The rate of increase is non-linear.

Thesis

ORIGINALITY REPORT

12%	%	12%	0%
SIMILARITY INDEX	INTERNET SOURCES	PUBLICATIONS	STUDENT PAPERS

PRIMARY SOURCES

1	G. Saxena, M. Kumawat, M. Kaushik, S.K. Jain, Mamta Aggarwal. "Bubble structure in magic nuclei", Physics Letters B, 2019 Publication	4%
2	G. Saxena, M. Kumawat, Mamta Aggarwal. "Anti-bubble effect of temperature & deformation: A systematic study for nuclei across all mass regions between A=20–300", Physics Letters B, 2018 Publication	1%
3	X. Chu, Y. Ni, G. Zhou. "Propagation of cosh-Gaussian beams diffracted by a circular aperture in turbulent atmosphere", Applied Physics B, 2007 Publication	1%
4	Manpreet Kaur, Abdul Quddus, Ankit Kumar, M. Bhuyan, S.K. Patra. "Effect of temperature on the volume and surface contributions in the symmetry energy of rare Earth nuclei", Nuclear Physics A, 2020 Publication	1%